Geological Society of America Bulletin

Metamorphic history of the central Himalaya, Annapurna region, Nepal, and implications for tectonic models

S.L. Corrie and M.J. Kohn

Geological Society of America Bulletin 2011;123, no. 9-10;1863-1879
doi: 10.1130/B30376.1

Metamorphic history of the central Himalaya, Annapurna region, Nepal, and implications for tectonic models

S.L. Corrie† and M.J. Kohn
Department of Geosciences, Boise State University, Boise, Idaho 83725, USA

ABSTRACT

Pressure-temperature-time (P-T-t) conditions of metamorphism have been determined in the Annapurna region of central Nepal that place new constraints on the structural and tectonic evolution of the Himalayan orogenic wedge. Peak P-T conditions increase structurally upward: ~525 °C and 8 kbar in the Lesser Himalayan sequence, 650 °C and 12 kbar at the base of the Greater Himalayan sequence across the Main Central thrust, 750 °C and 12 kbar in the middle of the Greater Himalayan sequence, and 775 °C and 13 kbar near the top of the Greater Himalayan sequence. Metamorphic monazite ages in the Greater Himalayan sequence also increase structurally upward: 16–21 Ma for subsolidus growth at the base of the Greater Himalayan sequence to ~25 Ma for peak-T metamorphism and anatexis near the top of the Greater Himalayan sequence. These ages are several million years older than at equivalent structural levels at Langtang, ~200 km to the east. The P-T-t data recommend reinterpretation of the Bhanuwa fault within the Greater Himalayan sequence as a thrust, and the presence of a different thrust structurally above the Bhanuwa thrust, here named the Sinuwa thrust. The new data are consistent with progressive stacking of tectonic slices, with calculated overthrust rates that are consistent with some (but not all) models that presume ~2 cm/yr convergence across the Himalaya since 25 Ma. Despite differences in absolute ages, similarities among the chemical systematics of monazite, peak P-T conditions, and overthrust rates calculated for Annapurna when compared to Langtang imply that the broad geodynamics in one part of an orogen can be realistically extrapolated within a few hundred kilometers, although the timing and duration of movement on discrete thrust surfaces may differ.

†E-mail: staceycorrie@boisestate.edu

INTRODUCTION

Syntheses of Himalayan tectonics indicate 400–700 km of shortening have been taken up across the Himalaya over the past 20–25 Myr (e.g., Yin and Harrison, 2000; DeCelles et al., 2001; Guillot et al., 2003; Robinson et al., 2006; Long et al., 2011). The implied average shortening rate, ~2 cm/yr, corresponds well with estimates of modern rates of shortening across the Himalaya (Bilham et al., 1997; Larson et al., 1999; Bettinelli et al., 2006). Yet despite decades of research, basic questions still remain about how strain was partitioned. Has the total convergence rate remained constant at ~2 cm/yr, or has it fluctuated significantly over time? How far can strain measurements and shortening rate estimates be extrapolated along strike? Was movement along the major faults in different regions contemporaneous, or was movement stalled in some areas while active in others? Thermal and mechanical models typically assume a constant shortening rate in the Himalaya since ~25 Ma (e.g., Bilham et al., 1997; Henry et al., 1997; Harrison et al., 1998; Huerta et al., 1998, 1999; Beaumont et al., 2001, 2004; Jamieson et al., 2002, 2004; Herman et al., 2010), but significant variations in the displacement rate on million-year time scales have been proposed in central Nepal (Kohn et al., 2004), and elsewhere within the Indo-Asian collision (Dunlap et al., 1998). Recognizing variations in displacement rates and timing requires a thorough assessment of the timing of peak metamorphism in successive tectonostratigraphic sections, the pressures and temperatures associated with the metamorphism, and the spatial relationship and proximity of the rocks to the shear zones.

To address these issues, samples were collected from a transect through the crystalline Himalaya along the Modi Khola in central Nepal, south of the Annapurna massif (Figs. 1 and 2). This transect has been mapped in detail (Hodges et al., 1996; Martin et al., 2005, 2007, 2010) and is located ~200 km west of a Langtang transect that has been studied intensively (Inger and Harris, 1992; MacFarlane, 1993, 1995; Fraser et al., 2000; Kohn, 2004, 2008; Kohn et al., 2004, 2005; Pearson and DeCelles, 2005) and therefore serves as a good basis of comparison. Martin et al. (2010) reported new P-T estimates for 13 Greater and Lesser Himalayan rocks along the Modi Khola, but did not offer them in a geochronological context. Pressure-temperature estimates have also been published from other transects through the central Himalaya of Nepal, including a transect along the Kali Ghandaki river to the west of the Modi Khola (Vannay and Hodges, 1996), and along the Marsyandi (Catlos et al., 2001; Beyssac et al., 2004) and Darondi (Kohn et al., 2001) rivers to the east between the Modi Khola and Langtang. To verify whether thrusting and convergence at Annapurna had the same rate, timing, and thermochemical evolution as at Langtang, which would indicate how far results from one area of an orogen can be extrapolated, we determined pressure-temperature conditions for 25 samples, age of peak metamorphism for four structural levels, and timing of movement along three major Himalayan thrusts. Ultimately, we evaluate the consistency of our P-T-t data against end-member models that presume 2 cm/yr shortening.

This work relies heavily on monazite crystallization ages. Monazite [(light rare-earth element [LREE], Y, Th)PO_4] is common in metapelites (Overstreet, 1967; see also review of Spear and Pyle, 2002), and is a popular chronometer in metamorphic rocks because of its high U and Th contents, very low initial Pb, and high retentivity of radiogenic Pb (e.g., see summaries of Parrish, 1990; Harrison et al., 2002). A critical step when employing monazite chronology is linking ages to corresponding metamorphic conditions via monazite chemistry. Numerous studies have shown the petrogenetic and tectonic value of this endeavor (e.g., Pyle and Spear, 1999, 2003; Ferry, 2000; Foster et al., 2000, 2002, 2004; Pyle et al., 2001, 2005; Spear and Pyle, 2002; Wing et al., 2003; Gibson et al., 2004; Kohn and Malloy, 2004; Dahl et al.,

GSA Bulletin; September/October 2011; v. 123; no. 9/10; p. 1863–1879; doi: 10.1130/B30376.1; 9 figures; 3 tables; Data Repository item 2011167.

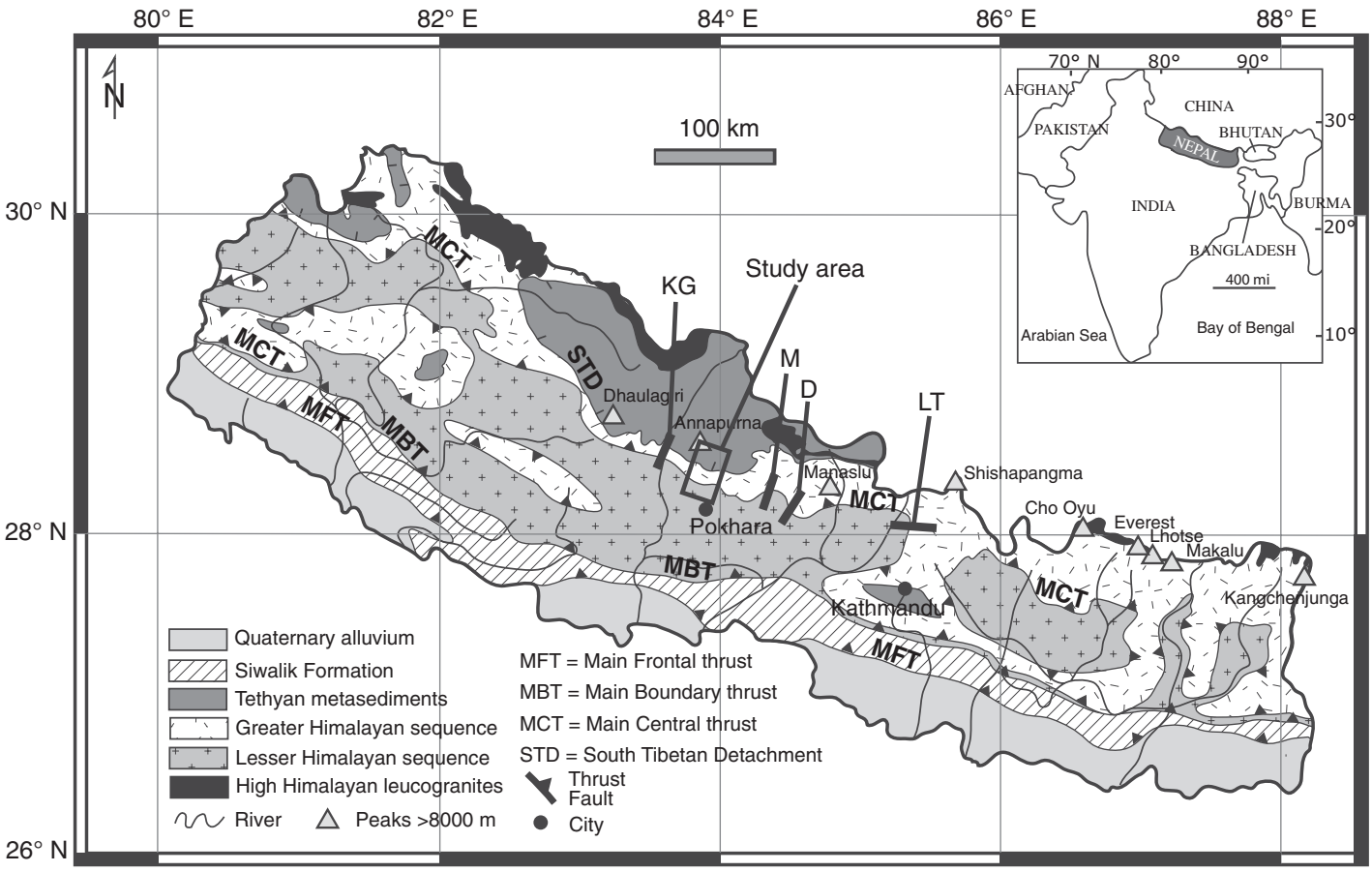

Figure 1. Generalized geologic map of Nepal illustrating the major tectonostratigraphic units (after DeCelles et al., 2004). Box indicates field area for this study. Location of other studies labeled for reference: LT—Langtang; D—Darondi; M—Marsyandi, KG—Kali Ghandaki.

2005; Kohn et al., 2004, 2005; Corrie and Kohn, 2008). By investigating these links, monazite ages may be assigned to specific points along the P-T path of a metamorphic assemblage, i.e., reflecting prograde, retrograde, or hydrothermal processes.

BACKGROUND

Geologic Setting

The high-grade metasedimentary rocks of the Greater Himalayan sequence form the metamorphic core of the Himalayan orogen, and in Nepal are commonly grouped into three formations: I, II, and III (LeFort, 1975; Colchen et al., 1986; Pêcher and Le Fort, 1986). Along the Modi Khola River in the Annapurna region of central Nepal, the lowest structural unit of the Greater Himalayan sequence, Formation I, consists of upper amphibolite-facies two-mica schist and migmatitic gneiss of generally pelitic composition. Formation II is composed of alternating beds of quartzite, marble, and pyroxene + amphibole-bearing calc-silicate. Formation III is a thin unit of pelitic schist and augen gneiss. In this study, we further divide Greater Himalayan sequence Formation I into three subgroups based on petrology. From structurally lowest to highest, these are 1a, 1b, and 1c. Formation 1a is muscovite rich and contains garnet that exhibits growth zoning and/or oscillations of major elements. Formation 1b rocks are locally migmatitic, and garnets have homogenous zoning. Formation 1c rocks are migmatitic with segregated leucosomes, and zoning in garnet shows chemically homogenous cores and near-rim increases in Mn.

Following Kohn et al. (2010), we divide the Lesser Himalayan sequence into two main units: the upper and lower Lesser Himalayan sequence. The lower Lesser Himalayan sequence generally consists of greenschist- to amphibolite-facies schists of the Paleoproterozoic Kuncha Formation, sporadically interleaved with orthogneisses of the Ulleri augen gneiss and overlain by clean, white quartzites of the Fagfog Formation. We define the upper Lesser Himalayan sequence as the mid to late Proterozoic (?) and Paleozoic metacarbonates and phyllites of the Dhading, Benighat, and Malekhu Formations plus the Paleozoic to Cenozoic slates, phyllites, and sandstones of the Tansen unit. Metamorphic grade in Lesser Himalayan sequence rocks along the Modi Khola River increases structurally upward toward the Main Central thrust, ranging from chlorite to garnet grade.

Generally speaking, the Main Central thrust is the ductile shear zone along which the Greater Himalayan sequence was thrust southward over the Lesser Himalayan sequence. Although the Main Central thrust figures heavily in tectonic reconstructions of the Himalaya (e.g., Yin, 2006 and references therein), the characteristics and location of the thrust are debated, stemming from various and disparate identifying criteria (Searle et al., 2008). The Main Central thrust has been mapped: (1) as a metamorphic contact near the kyanite isograd (e.g., Bordet, 1961; LeFort, 1975; Colchen et al., 1986); (2) as a lithological contrast between a distinctive quartzite and an overlying orthogneiss (Daniel et al., 2003); (3) by differences in Sr and/or Nd isotope compositions (Parrish and Hodges, 1996; Ahmad

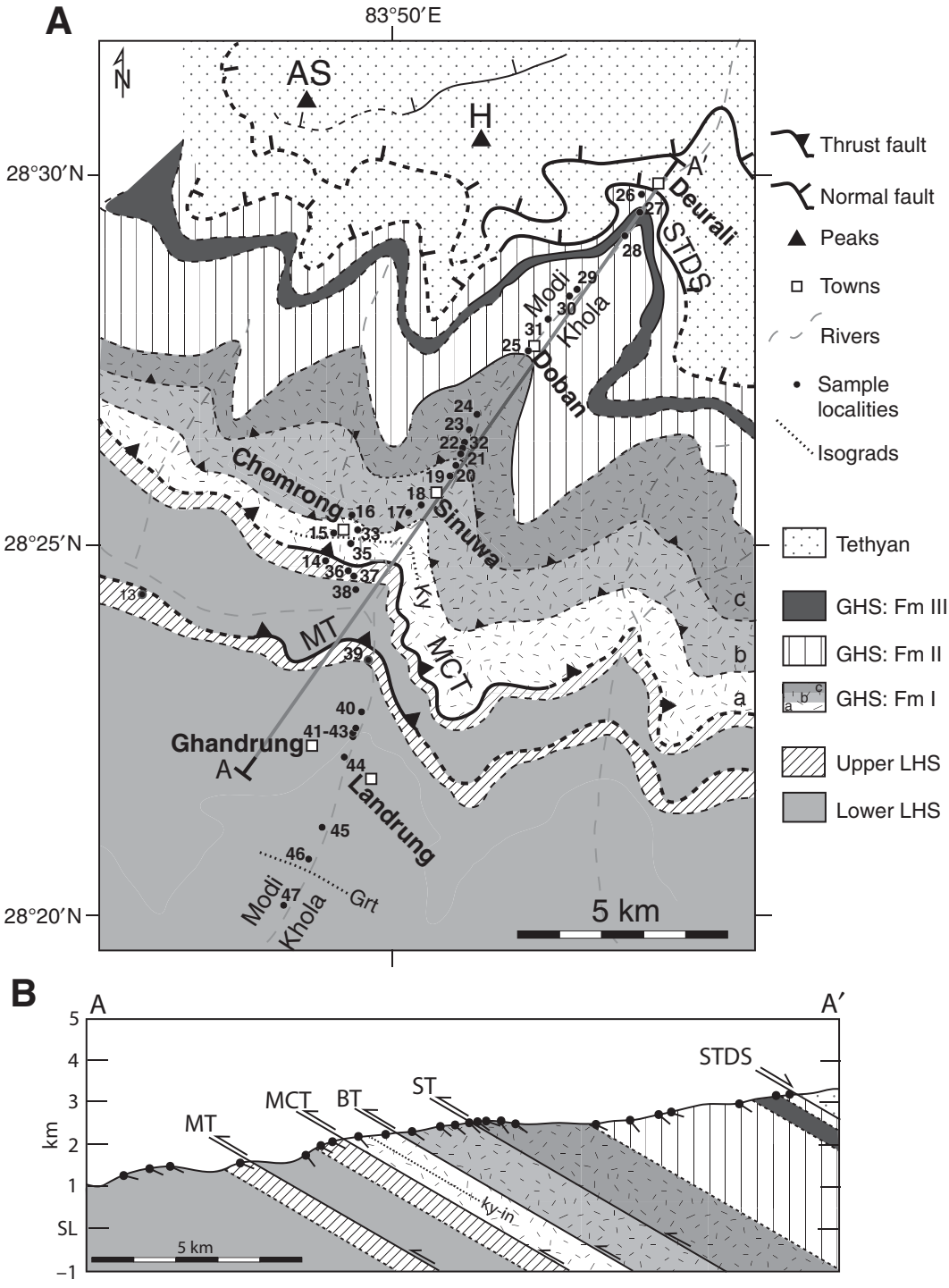

Figure 2. (A) Geologic map of the Annapurna region along the Modi Khola valley. Geology after Colchen et al. (1986), Hodges et al. (1996), Pearson and DeCelles (2005), and Martin et al. (2005, 2007). Numbers for sample locations follow the pattern AS01-xx. GHS—Greater Himalayan sequence; LHS—Lesser Himalayan sequence. Barbed lines represent thrust faults: MT—Munsiari thrust, MCT—Main Central thrust, BT—Bhanuwa thrust, ST—Sinuwa thrust. Single dashed lines are normal faults: STDS—South Tibetan detachment system. Labeled squares indicate towns. Black triangles are peaks: AS—Annapurna South, H—Hiunchuli. Dotted lines represent metamorphic isograds; Grt—garnet, Ky—kyanite. (B) Schematic cross section from A–A′, location shown in (A). Abbreviations as in (A).

et al., 2000; Robinson et al., 2001; Martin et al., 2005; Richards et al., 2005, 2006); (4) by differences in U-Pb detrital zircon ages (Parrish and Hodges, 1996; DeCelles et al., 2000); (5) by discrete metamorphic Th-Pb monazite ages and garnet zoning patterns (Harrison et al., 1997; Catlos et al., 2001, 2002; Kohn et al., 2004); (6) using strain indicators to find the maximum of a shear gradient (Martin et al., 2005; Searle et al., 2008); or (7) as a zone of high ductile strain up to 10 km thick that is bounded above and below by related thrusts (e.g., Catlos et al., 2001; Grujic et al., 2002; Searle et al., 2008). There are difficulties in using any one of these methods independently to define the Main Central thrust. General lithology, detrital zircons, and isotopic analysis provide information on stratigraphy, and mineral isograds and monazite ages provide information about metamorphic reactions. Ideally, one would map the Main Central thrust based on disproportionately large displacements relative to surrounding rocks. Yet variable rheological responses from different rock types, potential preexisting stratigraphic and tectonic structures, and strain recovery all obscure a clear location. Additionally, a lack of an obvious break in metamorphic grade

between the Lesser Himalayan sequence and Greater Himalayan sequence across the Main Central thrust makes it difficult to distinguish from field observations alone.

The juxtaposition of Greater Himalayan sequence and Lesser Himalayan sequence rocks is further complicated in Nepal by the presence of at least two major lithologic boundaries, interpreted as thrusts, that have both been mapped as the Main Central thrust (or MCT-I, MCT-II, upper MCT, lower MCT, etc.) at different structural and stratigraphic levels (see review of Yin, 2006). Where these two thrusts are distinguished, they are usually mapped where clear Greater Himalayan sequence rocks occur atop Lesser Himalayan sequence rocks (upper thrust), and where lower Lesser Himalayan sequence rocks occur atop upper Lesser Himalayan sequence rocks (lower thrust). Many workers restrict the name Main Central thrust to the upper thrust, and assign a different name to the lower thrust, either the Ramgarh thrust (e.g., DeCelles et al., 2000; Robinson et al., 2001) or the Munsiari thrust (e.g., Kohn, 2008). For this study, we assign the Main Central thrust to the Greater Himalayan sequence–Lesser Himalayan sequence contact, defined on a combination of lithologic, chemical, isotopic, and geochronologic criteria (Hodges et al., 1996; Martin et al., 2005, 2010), and show that it has taken up a disproportionately large component of thrust transport. We use the term Munsiari thrust for the structural contact between lower Lesser Himalayan sequence above upper Lesser Himalayan sequence. All thrusts are thought to sole into a long-lived master thrust surface, the Main Himalayan thrust.

Chronologically speaking, initial movement on the Main Central thrust was generally viewed as being ~20–22 Ma based on hornblende $^{40}Ar/^{39}Ar$ and monazite U-Pb ages (Hubbard and Harrison, 1989; Hodges et al., 1996; Johnson et al., 2001). However, more recent work has suggested later initial movement on the Main Central thrust in central Nepal and possibly Bhutan at 16 ± 1 Ma, with crystallization of in situ melts during Main Central thrust motion by 13 Ma (Daniel et al., 2003; Kohn et al., 2004, 2005).

PETROGRAPHY AND PETROLOGY

Mineral Assemblages

Lesser Himalayan sequence metapelites are generally characterized by the mineral assemblage Qtz + Ms ± Pl ± Bt ± Grt ± Chl, with accessory apatite + tourmaline + zircon ± ilmenite ± allanite ± magnetite. Two samples from one location contain chloritoid. Lesser Himalayan sequence calc-silicate rocks also contain hornblende and calcite. The foliation in rocks below the Munsiari thrust is defined primarily by muscovite and chlorite. Further upsection, from 500 m below the Munsiari thrust to the Main Central thrust, biotite and muscovite define the primary foliation and the mode of prograde chlorite decreases until it disappears altogether.

The mineral assemblage of Greater Himalayan sequence Formation I pelitic rocks is predominantly Qtz + Pl + Bt ± Ms ± Grt, with accessory apatite + tourmaline + zircon ± rutile ± monazite ± staurolite ± xenotime ± epidote. More calcic beds additionally contain hornblende, chlorite, and clinozoisite. Although several samples contain kyanite, AS01-22a is the only sample that contains sillimanite, which is locally developed as fibrous mats along quartz-plagioclase and plagioclase-plagioclase grain boundaries (cf. Kaneko, 1995), and is likely metasomatic (e.g., Vernon, 1979).

The calc-silicates and calcic quartzites from Greater Himalayan sequence Formation II contain the assemblage Qtz + Pl + Hbl ± Grt ± Ms, with accessory calcite + clinopyroxene + apatite ± titanite ± clinozoisite ± zircon ± potassium feldspar ± epidote. Formation II amphibolites have the assemblage Qtz + Pl + Hbl + Cpx ± Grt ± Chl, with accessory apatite ± titanite ± zircon ± calcite ± epidote (GSA Data Repository Table DR1[1]).

Mineral Chemistry

X-ray maps of Lesser Himalayan sequence garnet below the Munsiari thrust show smooth, major-element zoning (Fig. 3). Grossular and spessartine contents decrease from core to rim, whereas almandine and pyrope increase, as expected for prograde garnet growth (Spear et al., 1990). Additionally, some Lesser Himalayan sequence garnets below and above the Munsiari thrust display S-shaped or snowball inclusion textures that consistently indicate top-to-the-SSW shearing (Hodges et al., 1996; Fig. DR2 [see footnote 1]).

Garnet from rocks within 500 m of the Main Central thrust (above and below) retains primary growth zoning patterns (Fig. 3). Oscillatory zoning of calcium has been observed in garnet near the Main Central thrust in the Darondi and Langtang regions of central Nepal (Kohn et al., 2001, 2005; Kohn, 2004) and was proposed to result from heterogeneous thrusting and heating rates along the Main Central thrust (Kohn, 2004).

[1]GSA Data Repository item 2011167, Complete sample locations, mineral assemblages, chemical compositions, and photomicrographs, is available at http://www.geosociety.org/pubs/ft2011.htm or by request to editing@geosociety.org.

Garnet X-ray maps from Greater Himalayan sequence Formation I samples indicate increasing diffusional modification structurally upward. This is typical in high-grade metamorphic rocks (e.g., Florence and Spear, 1991), and was reported previously in this transect (Kaneko, 1995; Martin et al., 2010), and in the Marsyandi and Langtang regions of central Nepal (Catlos et al., 2001; Kohn et al., 2001, 2004). In Formation 1b, garnet zoning profiles are flat, consistent with diffusional homogenization. Higher upsection in Formation 1c, garnets display homogenous cores and increasing Mn toward rims, consistent with initial diffusional homogenization, followed by resorption and back diffusion during cooling (Florence and Spear, 1991; Spear, 1993; Kohn and Spear, 2000).

Plagioclase grains in almost all rocks show core-rim zoning with higher-Ca cores and lower-Ca rims. This is expected from garnet growth and fractional crystallization, as garnet growth depletes the matrix in Ca (Spear et al., 1990).

THERMOBAROMETRY

Rocks from the Modi Khola valley show chemical and textural evidence for only one episode of metamorphism, and display the familiar apparent inverted metamorphism associated with the Main Central thrust. Metamorphic grade increases progressively from biotite and garnet grade in the Lesser Himalayan sequence up to at least kyanite grade in the Greater Himalayan sequence (Fig. 2). The Appendix includes calibrations used and methods by which we infer the compositions that most closely approximate peak conditions. Overall, P-T conditions increase both in T and P from 500 to 525 °C and 7–8 kbar to ~575 °C and ~12 kbar, then increase in T to ~775 °C at nearly constant P (Fig. 4A). This convex upward distribution of P-T conditions is also documented at Langtang (Kohn, 2008).

With respect to structural position, rocks below the Munsiari thrust experienced peak metamorphic conditions of ~500–525 °C and 7.5 ± 1 kbar (Table 1 and Fig. 3). The similarity in Lesser Himalayan sequence P-T conditions over ~2 km structural distance plausibly results from in-sequence thrusting involving small-scale thrusts in a duplex (Kohn, 2008). Such data argue against a static metamorphic overprint associated with thrusting on the Main Central thrust alone (i.e., the "hot-iron" model of LeFort, 1975). Within the Munsiari thrust sheet, average temperatures and pressures of 550 ± 25 °C and 10.5 ± 1 kbar are 25–50 °C lower than inferred by Martin et al. (2010) at Annapurna and by Kohn (2008) for the same structural level at

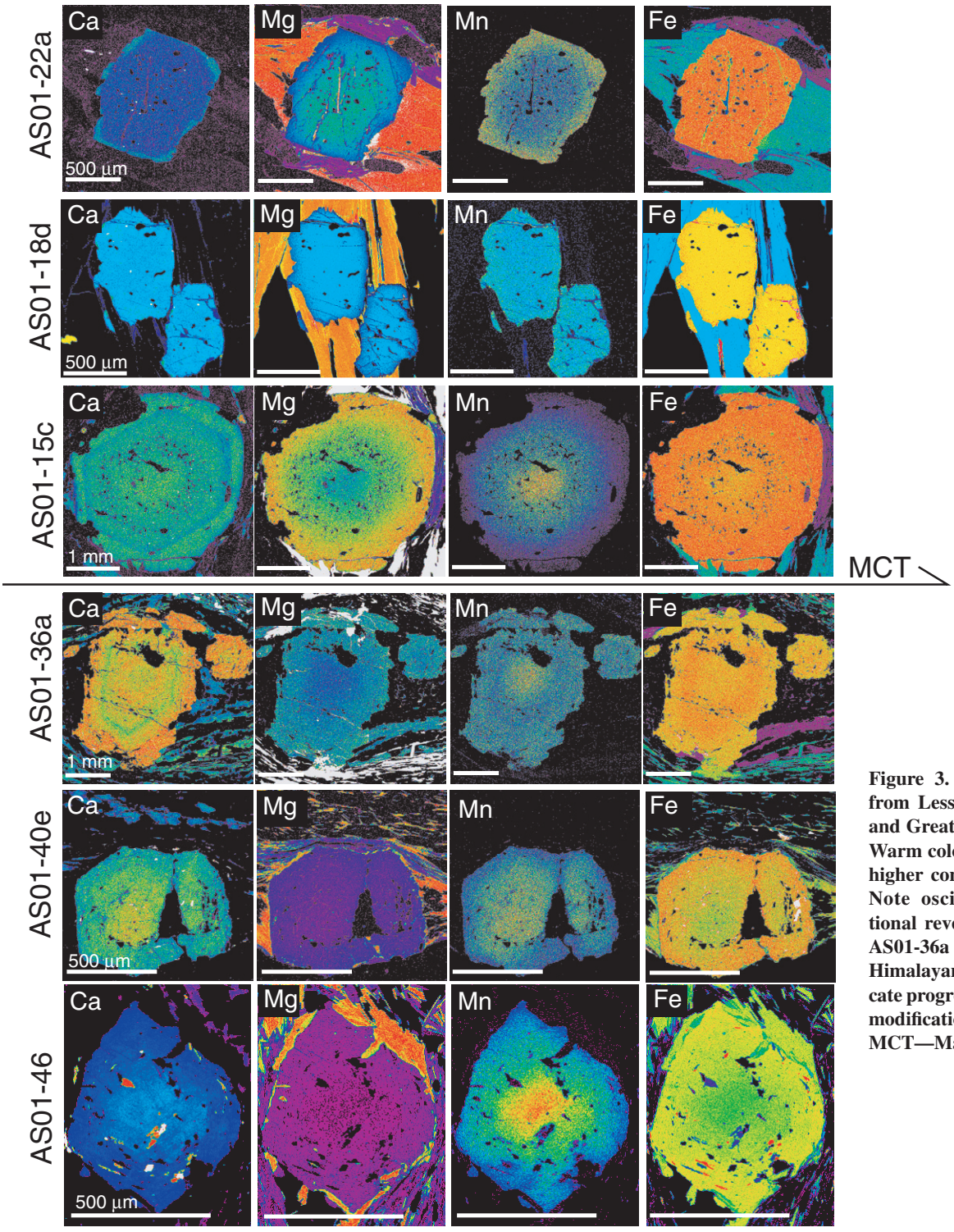

Figure 3. X-ray maps of garnet from Lesser Himalayan sequence and Greater Himalayan sequence. Warm colors (yellow-red) indicate higher concentrations of element. Note oscillations and compositional reversal for Ca and Mn in AS01-36a and AS01-15c. Greater Himalayan sequence samples indicate progressively more diffusional modification structurally upward. MCT—Main Central thrust.

Langtang, but slightly higher than those reported by Beyssac et al. (2004) for Annapurna.

Peak temperature and pressure conditions increase markedly across the Main Central thrust (Fig. 4) to 650 ± 25 °C and 12.0 ± 0.5 kbar, similar to data reported from the hanging wall of the Main Central thrust in the Annapurna region (Kaneko, 1995) and in the Marsyandi, Darondi, and Langtang regions of central Nepal (Catlos et al., 2001; Kohn et al., 2001, 2004; Kohn, 2008), but 50–100 °C and 2–3 kbar lower than the P-T conditions reported by Martin et al. (2010) for the same transect. Pressure-temperature conditions increase monotonically but nonlinearly upsection, consistent with production of an inverted metamorphic gradient via in-sequence thrusting, reaching 725–750 °C and 12.5 ± 1 kbar in the middle of Formation I (Formation 1b), 775 ± 20 °C and 12.5 ± 1 kbar at the top of Formation I (Formation 1c), and 775–800 °C and 13.5 ± 1 kbar in Formation II

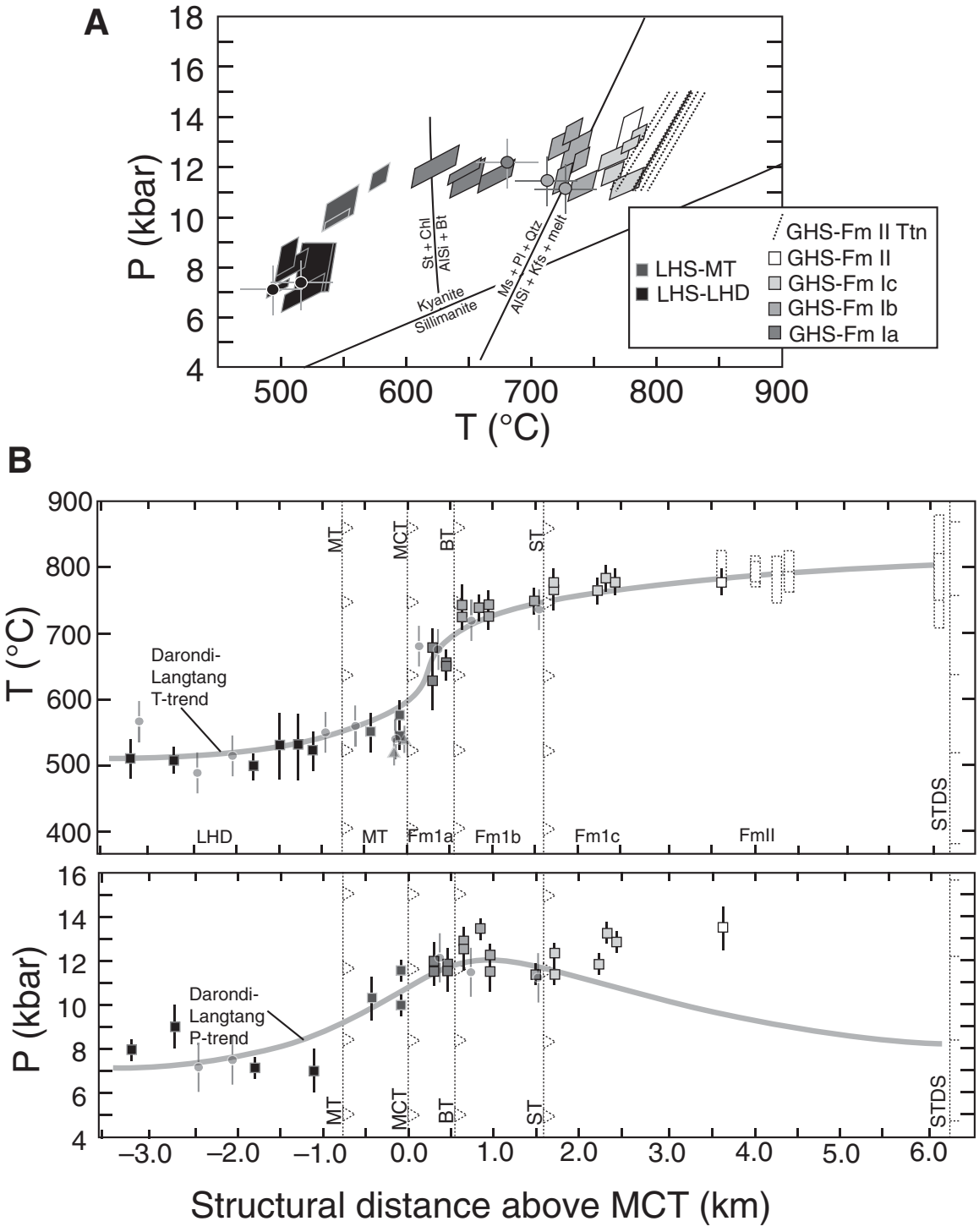

Figure 4. (A) Pressure (P) versus temperature (T) plot for rocks collected along the Modi Khola transect showing convex upward distribution. (B) Temperature and pressure versus structural distance from Main Central thrust (MCT). Temperatures show a strong gradient across the MCT and Bhanuwa thrust (BT), then a gradual increase structurally upward. Pressures are typically high, show a strong gradient across the Munsiari thrust (MT), then flatten to near-constant values structurally upward. Gray line represents T- and P-distance trend from transects in the Langtang and Darondi regions of Nepal (Kohn et al., 2001; Kohn, 2008). The T profile from this study corresponds well with those collected elsewhere in Nepal, but the P profile from this study does not show the decrease in pressures structurally upward as seen at Langtang. Triangles and circles represent P-T data from Beyssac et al. (2004) and Martin et al. (2010; recalculated using same methods as this study), respectively. Two analyses were omitted from the Martin et al. (2010) data set due to doubts about equilibration. Pressure-temperature conditions from Kaneko (1995) could not be recalculated because mineral compositions were not reported. GHS—Greater Himalayan sequence; HS—Lesser Himalayan sequence; LHD—Lesser Himalayan detachment; ST—Sinuwa thrust.

TABLE 1. THERMOBAROMETRIC RESULTS FROM ROCKS ALONG THE MODI KHOLA, ANNAPURNA REGION, CENTRAL NEPAL

Sample	Temperature (°C)	Pressure (kbar)	Garnet radii (mm)	Structural distance to Main Central thrust (km)
GHS Fm II				
AS01-26b	785 ± 35†		n.p.	6.10
AS01-26a	795 ± 90†		n.p.	6.10
AS01-29-1	805 ± 20†		450	4.40
AS01-29	775 ± 15†		n.p.	4.40
AS01-30a	780 ± 35†		n.p.	4.25
AS01-31c	790 ± 15†		n.p.	4.00
AS01-31b	790 ± 25†		1050	4.00
AS01-25	800 ± 25†		2100	3.60
AS01-25a	775 ± 20*	13.5 ± 1.0*	1900	3.60
Average	*790*	*13.5*		
GHS Fm Ic				
AS01-24a	775 ± 20*	13.0 ± 0.5*	500	2.45
AS01-23	780 ± 20*	13.0 ± 0.5*	650	2.35
AS01-32	765 ± 20*	12.0 ± 0.5*	1100, 900	2.25
AS01-20c	765 ± 30*	12.5 ± 0.5*	500	1.70
AS01-20a	775 ± 20*	11.5 ± 0.5*	300, 450	1.70
Average	*775*	*12.5*		
GHS Fm Ib				
AS01-19c	745 ± 20*	11.5 ± 0.5*	500, 400	1.50
AS01-18d	725 ± 20*	11.5 ± 1.0*	350, 300	0.95
AS01-18b	740 ± 20*	12.0 ± 0.5*	550	0.95
AS01-17b	735 ± 20	13.5 ± 0.5	300	0.80
AS01-16b	725 ± 20*	13.0 ± 0.5*	500, 400	0.65
AS01-16a	740 ± 30	12.5 ± 1.0	900, 600	0.65
Average	*735*	*12.5*		
GHS Fm Ia				
AS01-33b	650 ± 20	11.5 ± 1.0	400, 700	0.45
AS01-33a	645 ± 20	12.0 ± 0.5	550	0.45
AS01-15c	670 ± 30	11.5 ± 0.5	400, 1500	0.30
AS01-15a	625 ± 40	12.0 ± 1.0	600	0.30
Average	*650*	*12.0*		
Munsiari thrust sheet				
AS01-36b	575 ± 20	11.5 ± 0.5	500	–0.10
AS01-36a	545 ± 20	10.0 ± 0.5	950, 1100	–0.10
AS01-38b	550 ± 30	10.5 ± 1.0	350, 350	–0.40
Average	*555*	*10.5*		
Lesser Himalayan duplex				
AS01-40e	515 ± 30	7.0 ± 1.0	400	–1.10
AS01-41b	530 ± 50§		700, 600	–1.30
AS01-43a	530 ± 50§		1050	–1.50
AS01-44a	500 ± 20	7.0 ± 0.5	300	–1.80
AS01-45a	505 ± 20	8.5 ± 1.0	300, 350	–2.75
AS01-46	510 ± 30	8.0 ± 0.5	450, 350	–3.20
Average	*515*	*7.5*		

Note: All temperatures and associated errors rounded to nearest 5 °C, pressures and associated errors to 0.5 kbar. All temperatures calculated via garnet-biotite thermometry except AS01-41b, which was calculated via garnet-chlorite thermometry. Pressures calculated from garnet-plagioclase-muscovite-biotite, garnet-plagioclase-kyanite-quartz, and garnet-plagioclase-biotite-quartz barometry. n.p.—not present.

*Biotite corrected for retrograde net transfer reactions.

†Calculated by Zr-in-titanite thermometry; pressure assumed to be 12 kbar. Note that all samples contain zircon (except possibly AS01-25) and quartz, but not rutile.

§Temperature calculated at an assumed pressure of 8 ± 1 kbar.

(Table 1 and Fig. 4). Our Zr-in-titanite temperatures appear to be the first reported for Himalayan calc-silicates, and reinforce sparser temperature estimates from other lithologies. A discrete jump in temperatures is evident across the Bhanuwa thrust and probably also the Main Central thrust and Sinuwa thrust, consistent with juxtaposition of metamorphically distinct thrust sheets. Thermobarometric uncertainties and the distribution of samples, however, do permit smoother P-T transitions across the Main Central thrust and Sinuwa thrust (Fig. 4B). Martin et al. (2010) reported similar P-T conditions for Formations 1a and 1b.

Most differences between our P-T conditions and those reported by Martin et al. (2010) probably result from different thermobarometer calibrations. Application of our preferred calibrations using their tabulated compositions yields similar P-T conditions to results presented here (Fig. 4). Although Martin et al. (2010) do not specify their biotite solution model, which may contribute to P-T discrepancies, we especially note that they corrected garnet-biotite temperatures upward by several tens of degrees for biotite F-contents. Such a correction does not appear warranted for two reasons. First, garnet-biotite temperatures calculated for compositionally similar (low-F) biotite show no effect of F (Spear and Markussen, 1997). Second, Martin et al.'s preferred garnet solution model (Ganguly et al., 1996) may implicitly account for F in biotite because it was in part based on garnet-biotite Fe-Mg partitioning in natural rocks. That is, Martin et al. (2010) may consistently overestimate temperature. Of the two most discrepant samples, Martin et al. (2010) further suggest at least one may be out of equilibrium.

MONAZITE

Monazite Petrogenesis

Monazite is a common accessory in metapelitic Greater Himalayan sequence rocks and is typically zoned in thorium (Th) and yttrium (Y), reflecting reactions among the major silicates (Pyle and Spear, 1999, 2003; Wing et al., 2003; Kohn and Malloy, 2004; Kohn et al., 2005; Corrie and Kohn, 2008). As monazite grows, it preferentially fractionates Th, so younger prograde monazite typically has lower Th contents (Kohn and Malloy, 2004). Allanite also hosts Th, and although allanite is the primary LREE-accessory phase in the Lesser Himalayan sequence, it was found in only one Greater Himalayan sequence rock—a quartzite with a calcite cement. Monazite also sequesters Y, but so do other minerals including garnet, allanite, and xenotime (Spear and Pyle, 2002), potentially complicating interpretation of Y systematics. No evidence exists for prograde allanite or xenotime in any of the monazite-bearing Greater Himalayan sequence rocks. Garnet X-ray maps of Y do not indicate growth in the presence of xenotime, although a few samples contain minor retrograde (?) xenotime that is texturally associated with monazite rims. Yttrium systematics in most samples thus depend principally on the interplay between garnet and monazite (Pyle and Spear, 1999, 2003; Pyle et al., 2001). During prograde growth, Y is incorporated into garnet, so concentrations of Y in monazite should decrease with progressively higher grade. This simple trend changes during partial melting (normally via muscovite dehydration-melting), where monazite begins to dissolve, erasing direct chemical or chronological evidence of peak metamorphic temperatures. However, this reaction liberates Y to the melt (Spear and Pyle, 2002), where, upon cooling and melt crystallization, it is incorporated in relatively high concentrations in

re-growing monazite (Pyle and Spear, 2003; Kohn et al., 2004, 2005). Thus, post-anatectic rims of monazite should be chemically distinct (high-Y and possibly high-Th) from monazite that grew along the prograde path (Pyle and Spear, 2003; Kohn et al., 2004, 2005). That is, Th and Y systematics in monazite allow specific zones and ages to be chemically correlated within P-T space (Spear and Pyle, 2002; Pyle and Spear, 2003; Foster et al., 2004; Kohn et al., 2004, 2005).

Monazite Chemistry and Th-Pb Geochronology

Concentrations of ThO_2 and Y_2O_3 in Himalayan monazites from two Greater Himalayan sequence rocks range from 3.2 to 8.1 wt% and 0.5 to 2.8 wt%, respectively. Most Greater Himalayan sequence monazite grains show substantial Th and Y zoning. As expected due to Th fractionation, grains from several samples display a rimward decrease in Th. Many grains exhibit low-Y cores and higher-Y rims, but others have either relatively homogenous Y distributions or mottled Y zoning patterns. These different zones were targeted for in situ ion microprobe analysis to chemically link (wherever possible) each zone and its corresponding age.

Monazite from Greater Himalayan sequence Formation 1a contains mottled Y and Th zoning and no distinct high-Y rims that would indicate partial melting, consistent with calculated sub-anatectic P-T conditions (Figs. 3 and 4; Table 2). The 21–25 Ma ages from these grains thus represent prograde metamorphism. One monazite from sample AS01-15b contains evidence for an inherited component, with a low Y and Th core and anomalously old, probably mixed ages (47–114 Ma) that are not interpretable within the context of the Indo-Asian collision. Monazite with 400–500 Ma ages has been documented in the Greater Himalayan sequence (Catlos et al., 2002; Gehrels et al., 2003, 2006; Kohn et al., 2005; Martin et al., 2007), thus accounting for the inherited component noticed in a few of the monazites in this study. Multiple origins of these older grains are possible (Kohn et al., 2005).

Formation 1b monazite displays either distinct low-Y cores and high-Y rims that are attributable to partial melting (consistent with P-T conditions at or above the muscovite dehydration-melting reaction; Fig. 4), or indistinct zoning that is nevertheless geochronologically inhomogeneous (Fig. 5 and Table 2). Low-Y, prograde core ages are 24–29 Ma, although one monazite from AS01-16a has an age of 33 Ma, presumably the result of early prograde growth. Ages for postanatectic, high-Y rims are 17–22 Ma. Monazite from sample AS01-17b does not contain well-defined cores with overgrowth rims; rather, these monazites exhibit slight rimward Th decreases, and relatively flat and high Y. These relatively young (~18 Ma) monazite grains are interpreted to have grown entirely during postanatectic cooling. Martin et al. (2007) also analyzed monazite from Formation 1b, but only three grains were chemically characterized, and two contain obvious inheritance. The younger Th-Pb ages (~20 and 30 Ma) are within the range reported here.

Monazite from Formation 1c generally has low-Y cores and high-Y rims, the product of prograde growth and postanatectic cooling, respectively (Fig. 5 and Table 2). Such zoning is again consistent with calculated P-T conditions above muscovite dehydration-melting (Fig. 4). One grain from sample AS01-32 contains mottled zoning and slightly older ages, representing early prograde growth. Postanatectic cooling and monazite growth occurred 19–22 Ma—the age of high-Y rims and small homogenous high-Y monazites.

Monazite from Greater Himalayan sequence Formation III, just below the South Tibetan detachment, exhibits either mottled zoning, or slight rimward Th decreases. There is no evidence for rim growth associated with cooling after melting (Fig. 5 and Table 2). Higher Th zones in the monazite are 35–38 Ma and are

TABLE 2. ION-MICROPROBE AGE ANALYSES OF MONAZITE

Sample	Age (Ma) (± 2σ)	Comment	Sample	Age (Ma) (± 2σ)	Comment
AS01-35			AS01-19c		
1-1	21.6 ± 2.6	Low-Y	3-1	19.8 ± 1.0	Intermediate-Y
AS01-15b			3-2	20.1 ± 0.9	Low-Y
1-1	25.5 ± 2.1	Mottled Y, Th	3-3	18.1 ± 0.9	High-Y rim
4-1	113.7 ± 5.5	Mixed	3-4	20.9 ± 0.9	Intermediate-Y
4-2	47.0 ± 2.1	Mixed	3-5	19.3 ± 0.9	Intermediate-Y
5-1	24.3 ± 1.3	Mottled Y, Th	5-1	27.5 ± 1.1	Low-Y
5-2	25.3 ± 1.5	Mottled Y, Th	5-2	18.5 ± 0.8	High-Y rim
AS01-33b			5-3	22.9 ± 1.0	Mixed date
1-1	21.7 ± 1.0	Mottled Y, Th	5-4	20.8 ± 1.0	Intermediate-Y
1-2	23.1 ± 1.3	Mottled Y, Th	6-1	16.9 ± 0.7	High-Y
4-1	22.1 ± 1.0	Mottled Y, Th	6-2	20.2 ± 0.4	Low -Y core
4-2	22.6 ± 1.3	Mottled Y, Th	7-1	20.8 ± 0.7	Intermediate-Y rim
5-1	21.3 ± 0.9	Mottled Y, Th	7-2	28.6 ± 0.8	Low-Y core
5-2	22.0 ± 1.0	Mottled Y, Th	7-3	19.8 ± 0.9	High-Y rim
AS01-16a			AS01-20a		
1-2	25.9 ± 1.2	Low-Y, Th core	1-1	21.7 ± 1.3	Intermediate-Y
1-3	24.9 ± 1.3	Intermediate-Y	1-2	26.8 ± 2.0	High-Y
3-1	25.7 ± 1.3	Intermediate-Y	3-1	93.6 ± 4.7	Inherited
3-2	18.7 ± 1.4	Intermediate-Y	5-1	74.7 ± 3.3	Inherited
3-3	25.3 ± 1.9	Intermediate-Y	5-2	22.7 ± 1.0	Mixed date
4-1	33.2 ± 2.0	Low-Y, Th core	AS01-22a		
4-2	25.7 ± 1.5	Intermediate -Y	1-1	178.9 ± 7.0	Inherited
4-3	27.2 ± 1.5	Low-Y, Th	3-1	20.9 ± 1.0	High-Y
AS01-16b			AS01-32		
1-1	20.3 ± 0.4	Mottled Y, Th	1-1	29.3 ± 1.4	Low-Y core
1-2	25.2 ± 0.4	Mottled Y, Th	3-1	25.0 ± 1.2	Mixed date
2-1	24.4 ± 0.4	Mottled Y, Th	3-2	29.1 ± 1.4	Low-Y core
2-2	27.0 ± 0.4	Mottled Y, Th	4-1	28.2 ± 0.4	Mottled Y, Th
3-1	25.4 ± 0.3	Mottled Y, Th	4-2	28.7 ± 0.4	Mottled Y, Th
3-2	19.8 ± 1.2	Mottled Y, Th	4-3	28.2 ± 0.4	Mottled Y, Th
4-1	26.0 ± 0.4	Mottled Y, Th	5-1	31.9 ± 1.0	High-Y
4-2	25.9 ± 0.4	Mottled Y, Th	5-2	31.5 ± 0.8	High-Y
4-3	26.1 ± 0.3	Mottled Y, Th	6-1	29.7 ± 0.4	Mottled Y, Th
AS01-17b			AS01-23		
2-1	17.9 ± 0.9	High-Y, Th	1-1	18.9 ± 1.0	High-Y rim
3-1	17.9 ± 1.8	High-Y, Th	1-2	23.1 ± 1.4	Low-Y core
AS01-18d			1-3	20.5 ± 1.0	Low-Y
1-1	25.6 ± 1.3	Mixed date	1-4	20.5 ± 1.2	High-Y rim
1-2	25.1 ± 1.5	Mixed date	2-1	20.0 ± 1.0	Low-Y
1-3	27.7 ± 1.7	Low-Y core	2-2	21.4 ± 1.0	Low-Y
4-1	29.5 ± 1.3	Low-Y core	5-1	20.3 ± 0.9	Low-Y
4-2	21.3 ± 1.2	High-Y rim	5-2	20.3 ± 1.1	Low-Y
4-3	19.7 ± 1.8	High-Y rim	AS01-27		
AS01-19c			1-1	32.7 ± 1.4	Mottled Y, Th
1-1	19.0 ± 0.7	High-Y	1-2	30.2 ± 1.5	Mottled Y, Th
1-2	18.7 ± 0.9	High-Y	3-1	36.7 ± 1.7	Mottled Y, Th
1-3	28.4 ± 1.2	Low-Y core	4-1	33.0 ± 1.5	Mottled Y, Th
1-4	24.9 ± 1.0	Mixed date	5-1	37.4 ± 1.3	Mottled Y, Th
2-1	27.4 ± 1.4	Low-Y core	5-2	34.2 ± 1.3	Mottled Y, Th
2-2	18.7 ± 0.8	Intermediate-Y rim	6-1	37.8 ± 3.3	Intermediate-Y
2-3	19.6 ± 1.1	Intermediate-Y	6-2	37.3 ± 3.0	Intermediate-Y
			6-3	37.2 ± 4.6	Intermediate-Y
			6-4	35.0 ± 4.0	Low-Y, Th rim

Note: All analyses contained 95% radiogenic ^{208}Pb or higher.

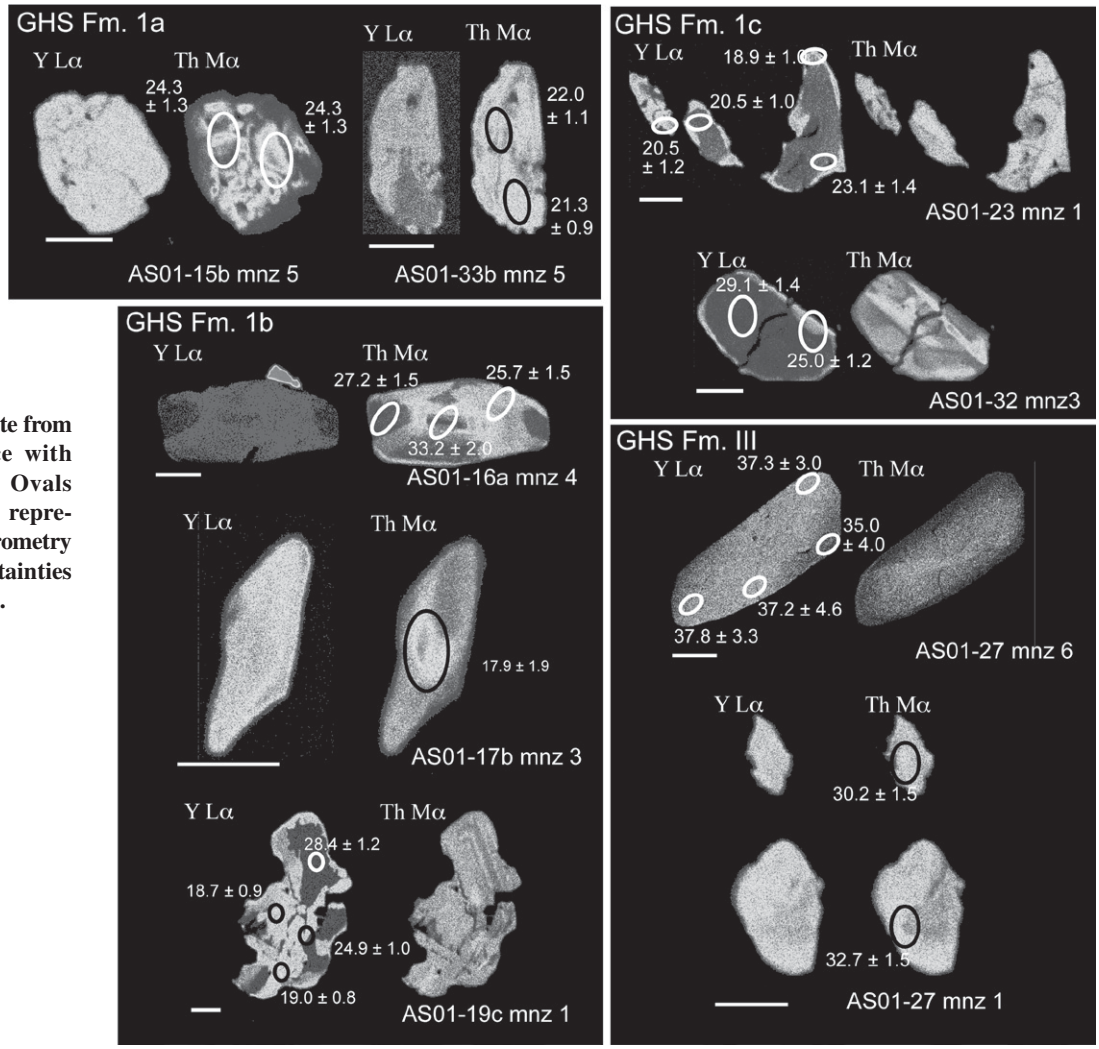

Figure 5. X-ray maps of monazite from Greater Himalayan sequence with ion-microprobe Th-Pb data. Ovals and their corresponding ages represent secondary ion mass spectrometry analysis spot locations. Uncertainties are 2σ; scale bars are all 50 μm.

ascribed to early prograde growth with later prograde growth represented by 30–35 Ma, mottled Y and Th zones.

With one exception in an arguably plutonic grain (Spear and Pyle, 2002; Fig. DR4 [see footnote 1]), we found no chemical, chronologic, or textural evidence for low-temperature growth or alteration of monazite, which is commonly indicated by anomalous Y, Th, or U contents and young ages (e.g., Kohn et al., 2005). Furthermore, muscovite $^{40}Ar/^{39}Ar$ cooling ages in the region indicate that the Main Central thrust sheet had cooled through muscovite closure (~400 °C; McDougall and Harrison, 1999) by 14–15 Ma (Vannay and Hodges, 1996); all monazite ages considered here are older.

Monazite Age Distribution

Four main generations of monazite have been identified in samples south of the Annapurna Range along the Modi Khola in central Nepal. From oldest to youngest they are: inherited and/or mixed, early prograde, late prograde, and postanatectic, and can be distinguished chemically or chronologically.

Age-probability diagrams for monazite (Fig. 6) show distinct peaks that correspond to specific chemistries, and thus to petrologic origins. Analyses that inadvertently covered two distinctly separate zones in the monazite were not used in the age-profile calculations. Particularly significant in anatectic rocks is the timing of the last growth of prograde monazite (youngest low-Y and -Th peak) versus the first instance of melt crystallization during cooling (high-Y overgrowth). Together, these ages bracket the timing of anatexis. Additionally, the diagrams demonstrate decreasing temperatures (presence or absence of anatexis) and ages of metamorphism structurally downward, consistent with progressive underplating of tectonic slices.

In the structurally highest rocks of the Formation III orthogneiss, the latest prograde monazites have an age of 30–33 Ma. Structurally lower in Formation 1c, the latest prograde subsolidus monazite formed 27–30 Ma (~3 Myr younger than Formation III), with crystallization of in situ melts 19–22 Ma. Direct dating of peak-T metamorphism is not possible in these rocks because monazite is consumed during partial melting. Peak-T metamorphism and anatexis thus probably occurred 24.5 ± 2.5 Ma in Formation 1c. Structurally lower rocks have the same chemically defined generations of monazite, but again displaced to younger ages and lower temperatures. Pre- versus postanatectic ages from Formation 1b are 29–24 Ma and 22–17 Ma, respectively, implying melting at 23 ± 1 Ma. That is, Formations 1b and 1c both underwent similar reactions (specifically prograde muscovite dehydration-melting and retrograde melt crystallization), but at different times. Monazite in Formation 1a experienced subsolidus growth from 21 to 16 Ma, the same time period during which Formation 1b was cooling.

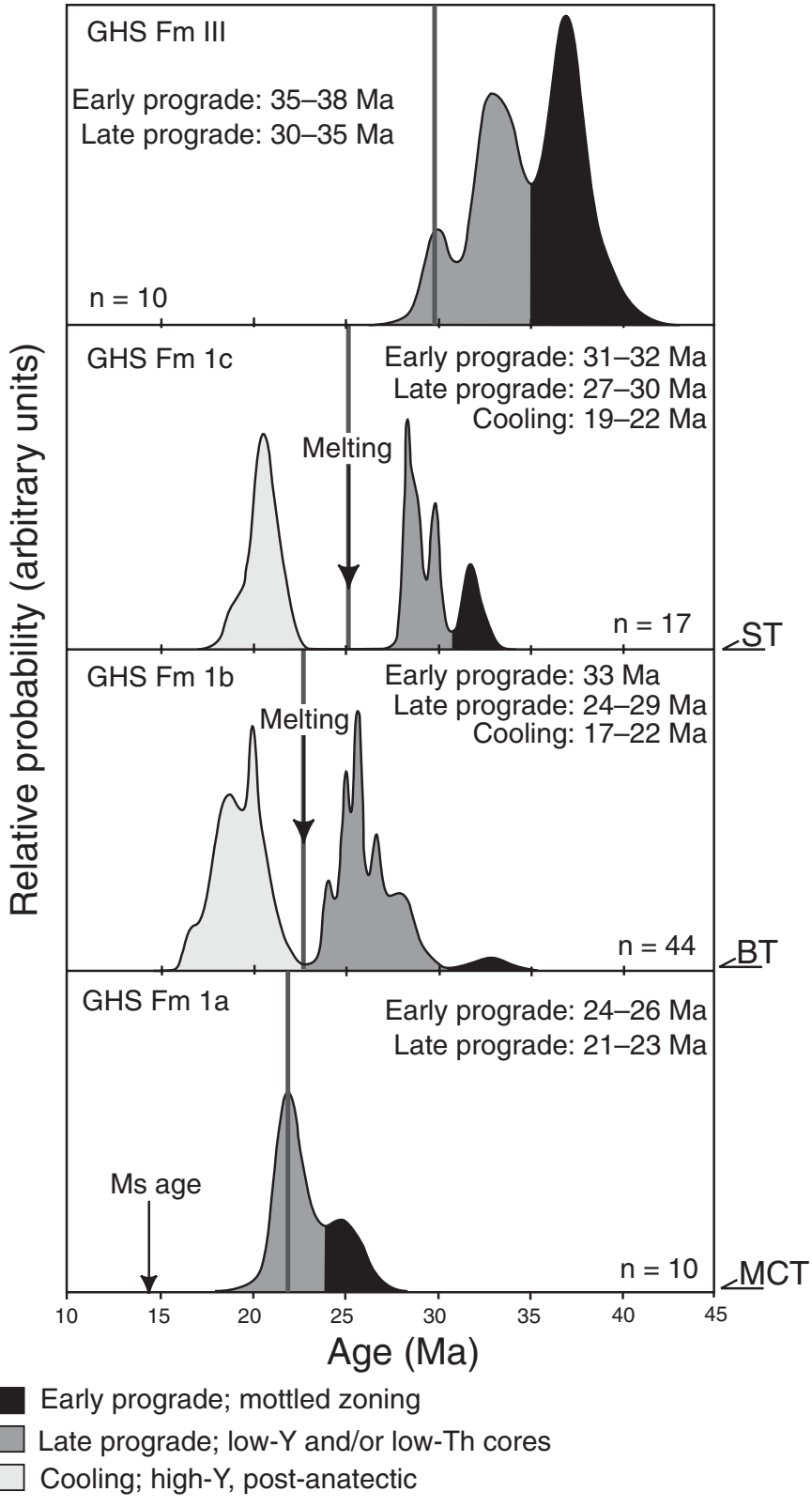

Figure 6. Probability distributions of monazite ages, distinguished according to monazite chemistry. Thick gray lines illustrate timing of peak metamorphism. Arrow in Greater Himalayan sequence Formation 1a box shows $^{40}Ar/^{39}Ar$ muscovite ages from the same structural level from the nearby Kali Gandaki valley (Vannay and Hodges, 1996). BT—Bhanuwa thrust; ST—Sinuwa thrust; MCT—Main Central thrust.

DISCUSSION

Local Structural Inferences

Martin et al. (2010) first interpreted the contact between Greater Himalayan sequence Formations 1a and 1b as a normal fault based primarily upon a 4 kbar pressure difference between hanging-wall and footwall rocks, and shorter retrograde diffusion profiles in garnet in footwall rocks. Pressure-temperature data from this study do not support this interpretation. Instead, our data indicate very little change in pressure across this boundary, but an ~85 °C increase in temperature (Table 1 and Fig. 4). This temperature increase can account for the longer retrograde diffusion profiles in the hanging wall versus the footwall. Pressure-temperature calculations and monazite geochronology do, however, support the presence of a fault in this location. Thus, we reinterpret the fault as a thrust, the Bhanuwa thrust.

Chronologic and thermobarometric differences among Greater Himalayan sequence rock units further suggest a thrust contact between Formations 1b and 1c (Fig. 2), which we name the Sinuwa thrust. The Sinuwa thrust emplaced high-T, pervasively migmatitic rocks of Greater Himalayan sequence Formation 1c atop slightly lower-T, locally migmatitic rocks of Formation 1b. Based on monazite geochronology (Fig. 6), initial melts may have formed in the Sinuwa thrust sheet (Formation 1c) as early as 27 Ma, but not until 23 Ma in the Bhanuwa thrust sheet (Fig. 6). The large gap between pre- and postanatectic monazite in the Sinuwa thrust sheet precludes pinpointing the timing of initial cooling. Possibly cooling commenced as early as 25–26 Ma, during heating of the Bhanuwa thrust sheet, and emplacement of the Sinuwa thrust. Alternatively, within uncertainty, the Sinuwa thrust and Bhanuwa thrust rocks could have been buffered at anatectic conditions until cooling and melt crystallization in both sheets at ~22 Ma. Afterward, the two sheets probably experienced similar cooling histories as they were transported together in the hanging wall of the Bhanuwa thrust. Presuming that cooling resulted primarily from thrust emplacement (Kohn et al., 2004; Kohn, 2008) rather than from erosion or vertical displacement (that is, the vertical uplift was quite small compared to the lateral displacement, e.g., 1–2 km vertical versus 50–80 km lateral; Fig. 7), these data imply initial Sinuwa thrust movement sometime between 22 and 27 Ma, and initial Bhanuwa thrust movement at 22 Ma. There may be other structures in the upper part of the Greater Himalayan sequence (e.g., between Formation I and II, or within

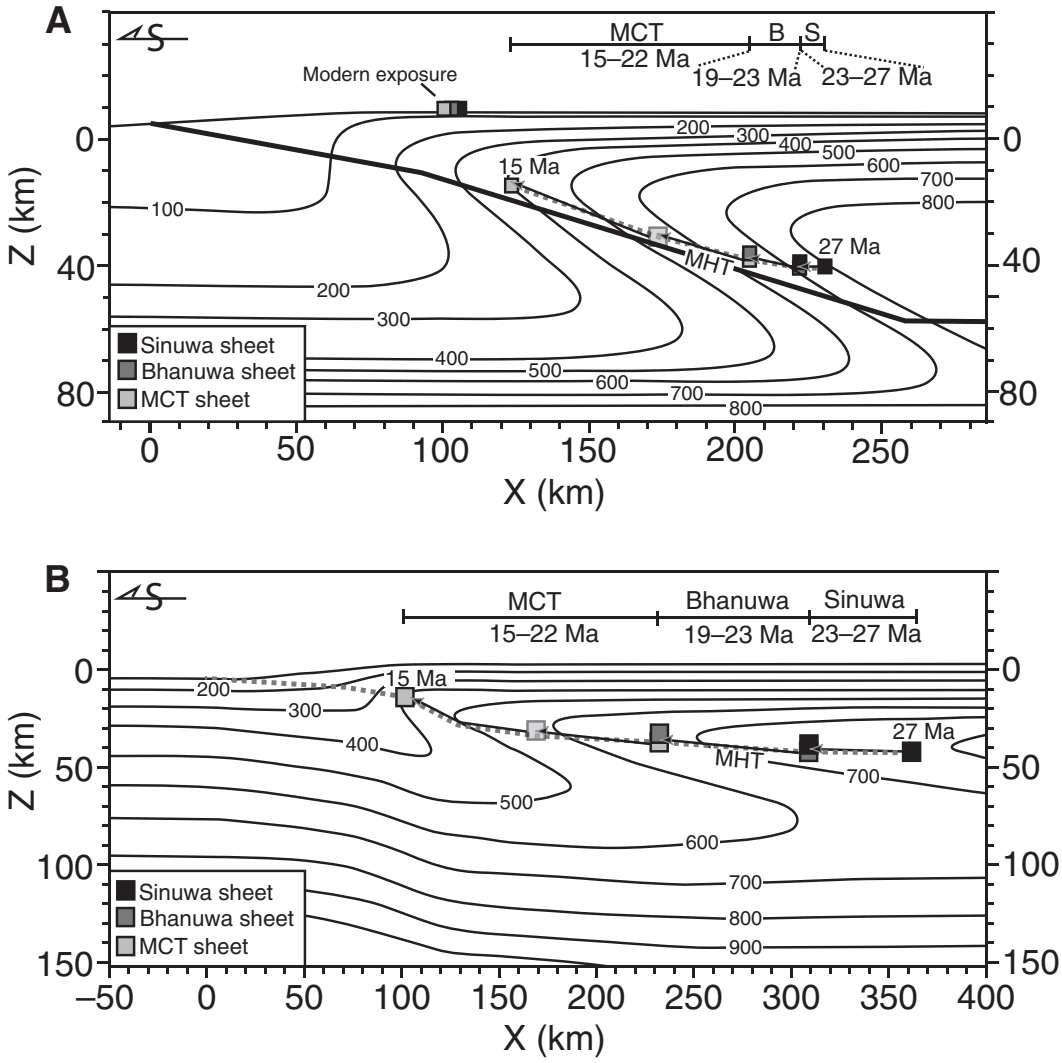

Figure 7. Schematic illustration of the displacements of different thrust packages in the context of the modern Main Himalayan thrust (MHT) and thermal models for the Himalaya. The location and timing of each spot is constrained by thermobarometric calculations, the thermal structure, and cooling ages determined by monazite or muscovite geochronology. X-axis values are relative to the surface expression of the active Main Frontal thrust; Z-axis values are relative to sea level. (A) Comparison to relatively hot model (Herman et al., 2010). (B) Comparison to relatively cold model (Henry et al., 1997; Bollinger et al., 2006). The Herman et al. (2010) model is consistent with petrologic and chronologic data, whereas the Henry et al. (1997) and Bollinger et al. (2006) models are not; see text for discussion. B—Bhanuwa; S—Sinuwa; MCT—Main Central thrust.

Formation II), but sampling was insufficiently dense to be definitive.

The Greater Himalayan sequence–Lesser Himalayan sequence contact has long been interpreted as a thrust (the Main Central thrust), most recently in the Annapurna region on the basis of strain gradients (Martin et al., 2005). As discussed by Kohn (2008), apparent temperature gradients provide an alternative means of assigning significance to local structures. Large temperature gradients or jumps, as exhibited across the Main Central thrust and Bhanuwa thrust at Annapurna, imply long-lasting displacement on a single shear zone, especially when coupled with small pressure differences. That is, the Main Central thrust and Bhanuwa thrust must represent specific major structures. Smaller temperature gradients, as exhibited within Formation II and the Lesser Himalayan sequence, imply successive underplating, with smaller thrust displacements on individual shears. We still group rocks within these sections based on lithology, petrology, and geochronology, but with the understanding that in detail numerous smaller shears likely occur. Pressure differences across the Main Central thrust and Munsiari thrust imply either a ramp in the décollement or progressive shallowing of the décollement between the time of the peak of metamorphism in the Main Central thrust sheet and in the Lesser Himalayan duplex (LHD).

Overthrust Rates

Overthrusting in a wedge is defined as the component of overall convergence that is accommodated by lateral movement of the hanging wall along the basal thrust relative to a fixed reference position on the thrust, such as the thrust front or ramp; at steady state, erosion or tectonic denudation balances overthrusting. Underthrusting is then the rate at which the footwall is thrust under the reference point. For movement on a single basal thrust, the sum of underthrusting and overthrusting equals the thrust rate. Within the context of a thermal model, rates of overthrusting can be calculated from thermobarometric and geochronologic data (Kohn et al., 2004). These calculations require that cooling in the hanging wall results from thrust juxtaposition against cold footwall rocks, rather than from erosion or displacement with a significant vertical component. This assumption is consistent with original gentle thrust orientations (e.g., DeCelles et al., 2001; Robinson et al., 2003), allowing these faults to accommodate significant convergence at depth (30–40 km depth; Fig. 7). In addition, where the Main Himalayan thrust is at such depths today, modern erosion directly above is <2 mm/yr (Lavé and Avouac, 2001). Finally, barometric estimates of footwall and hanging-wall rocks for most thrusts are not so different that vertical

exhumation due to tectonic denudation or vertical transport could have been the primary means of cooling. The Main Central thrust violates this assumption and is discussed in more detail below. The other key assumption is that only one thrust among the Sinuwa thrust, Bhanuwa thrust, and Main Central thrust may be active at any given time. This is also problematic (see below), but allows for limits to be placed on overthrust rates.

Overthrust rates were calculated using the method of Kohn et al. (2004). The minimum amount of cooling during fault slip was approximated based on the peak temperatures in the hanging wall and those in the footwall. Thermal models for the central Himalaya define temperature-depth distributions on which peak P-T data may be plotted, and allow ΔT's of cooling to be converted into transport distances (Fig. 7 and Table 3). Effectively, thermal models define lateral thermal gradients, from which ΔT's are converted to displacements. Peak metamorphic ages from monazite in different thrust sheets provide a maximum duration of thrust displacement. The overthrust rate is thus derived from the displacement distance divided by the time period of displacement. In reality, model differences and uncertainties in peak temperature and chronology propagate to large errors for calculated rates. Thus we mostly consider our results in terms of evaluating consistency (or not) with a nominal 20 mm/yr Himalayan convergence rate, partitioned into ~5–6 mm/yr overthrusting and exhumation of the Himalayan wedge, and 14–16 mm/yr underthrusting (Henry et al., 1997; Bollinger et al., 2006; Herman et al., 2010).

This approach cannot be applied directly to the Main Central thrust, because we cannot pinpoint both a depth and time of metamorphism of any associated rocks: the depth of metamorphism of the underlying Munsiari thrust sheet is known, but its timing is not, whereas the timing of cooling below muscovite closure is known (14–15 Ma, Vannay and Hodges, 1996), but its depth is not. The relatively small difference in pressure between the Main Central thrust and Munsiari thrust rocks and small vertical thermal gradient near the thrust plane in thermal models imply that the Main Central thrust sheet experienced at least 100 °C cooling at depth (Fig. 7A) within 7–8 Myr (between 22 and 14–15 Ma). Thermal models indicate a maximum of another 150 °C cooling on the Main Central thrust and/or lower thrusts to reach muscovite closure nearer the toe of the wedge (Fig. 7A). These observations provide broad limits on Main Central thrust displacement and rates: 100–250 °C cooling in 7–8 Myr.

The calculated overthrust rates depend critically on which thermal model one considers. Here we consider only steady-state models because they all share broadly similar thermal structures, albeit with different temperature gradients, whereas there are an infinite number of non–steady-state models. Our comparisons seek to establish the compatibility (or not) of petrologically calculated versus model overthrust rates. Noting that the calculated overthrust rate is a minimum because thrusting could be taken up on more than one structure, consistency versus inconsistency occurs when calculated overthrust rates are less than or equal to versus greater than model overthrust rates. The Bollinger et al. (2006) model, refined from Henry et al. (1997), is a relatively cold end member with widely spaced isotherms, mainly because it prescribes low mantle heat flux as a lower boundary condition. This model implies larger transport distances and faster overthrusting rates. In contrast, the Herman et al. (2010) model, which prescribes a relatively shallow 800 °C thermal boundary layer, and the high mantle heat flux model of Henry et al. (1997) are relatively hot end members, with closely spaced isotherms. These models imply shorter distances and slower overthrusting rates. In all models, our P-T data closely correspond to the assumed thrust plane (see also data of Kohn et al., 2004), and high-T chronologies instead discriminate best among models (Kohn, 2008).

Calculated overthrusting rates and a priori model predictions correspond best using the Herman et al. (2010) model: the overthrusting rate of the input model is 6 mm/yr, and our data imply rates of ≤4 mm/yr at 23–27 Ma (Sinuwa thrust), 4.5 ± 2 mm/yr at 19–23 Ma (Bhanuwa thrust), and 4–11 mm/yr at 15–22 Ma (Main Central thrust; Fig. 7A and Table 3). In contrast, the colder thermal models of Henry et al. (1997) and Bollinger et al. (2006) assume overthrusting rates of ~5 mm/yr, whereas our data then imply rates of 10–20 mm/yr, or two to four times too high (Fig. 7B and Table 3). Kohn et al. (2004) calculated similar ~20 mm/yr overthrusting rates based on P-T-t data at Langtang and the cooler models of Henry et al. (1997), and we now recognize the mutual incompatibility of these models and data. In contrast, the Herman et al. (2010) model generally predicts the Langtang data set well.

Overall, petrologic and chronologic data from both Annapurna and Langtang require relatively hot conditions to be consistent with a ~5 mm/yr overthrusting rate and 2 cm/yr convergence rate component across the Himalaya from ~25 to ~15 Ma (Herman et al., 2010; Fig. 7A). Cooler models (Henry et al., 1997; Bollinger et al., 2006) imply much faster overthrusting and overall convergence than are currently assumed (Fig. 7B). We prefer the hotter thermal models because the underthrusting rate is viewed as quasiconstant over the past 25 Myr (see summary of Herman et al., 2010), and we know no reason to suppose large variations in the partitioning of overthrusting versus underthrusting. However, our data then require additional mantle heat, for example possibly sourced by removal of the oceanic lithospheric slab and consequent asthenospheric upwelling (Kohn and Parkinson, 2002). We do not believe leucogranite intrusions are important heat sources in this area, because the only large plutonic complex, the Manaslu, is over 50 km away, and because local partial melts are already at thermal equilibrium, i.e., do not advect heat.

TABLE 3. ESTIMATES OF THRUST TEMPERATURES, TIMES, MINIMUM DISPLACEMENTS, AND DISPLACEMENT RATES

Thrust	Peak Temperature (°C)	Time (Ma)	Cooling temperature (°C)	Time (Ma)	Distance (km)	Rate (cm/yr)
Model A						
Sinuwa	775 ± 20	27 ± 1	735 ± 20	23 ± 1	8 ± 7	0.2 ± 0.15
Bhanuwa	735 ± 20	23 ± 1	650 ± 25	19 ± 2	18 ± 8	0.5 ± 0.2
Main Central (minimum)	650 ± 25	22 ± 1	555 ± 25	15 ± 1	30 ± 20	0.4 ± 0.3
Main Central (maximum)	650 ± 25	22 ± 1	400 ± 25	15 ± 1	75 ± 15	1.1 ± 0.3
Model B						
Sinuwa	775 ± 20	27 ± 1	735 ± 20	23 ± 1	55 ± 50	1.4 ± 1.3
Bhanuwa	735 ± 20	23 ± 1	650 ± 25	19 ± 2	85 ± 40	2.1 ± 1.5
Main Central (minimum)	650 ± 25	22 ± 1	555 ± 25	15 ± 1	60 ± 25	0.9 ± 0.4
Main Central (maximum)	650 ± 25	22 ± 1	400 ± 25	15 ± 1	130 ± 20	1.9 ± 0.5

Structural Implications

The similarity in inferred peak ages for the Sinuwa thrust, Bhanuwa thrust, and Main Central thrust could in principle indicate simultaneous initial cooling of all three sheets at ~22 Ma (Fig. 8, model 2). Because pressures appear to increase structurally upward slightly, such cooling could not occur in a single thrust with an inverted

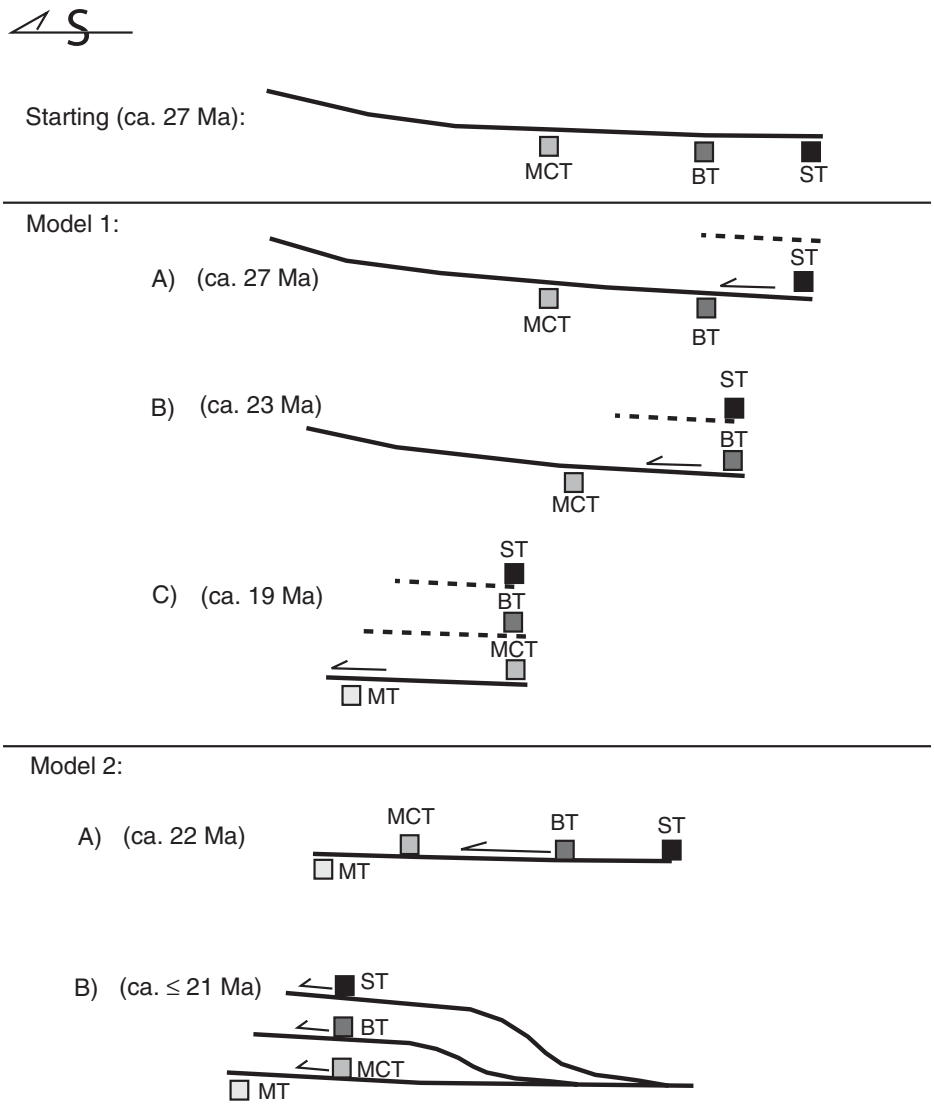

Figure 8. Schematic diagram showing two end-member models of thrust development. Model 1 exhibits in-sequence thrusting as the thrust plane cuts downsection. Model 2 shows initial cooling of all three thrust packages at ~22 Ma, followed by later out-of-sequence juxtaposition of the Bhanuwa thrust (BT) and Sinuwa thrust (ST). MCT—Main Central thrust.

thermal gradient. Rather, each rock package might have cooled during transport along the same basal thrust (the Main Himalayan thrust), with later juxtaposition of already-cooled rocks along the Sinuwa thrust and Bhanuwa thrust. That is, this model implicitly requires many tens of km of out-of-sequence thrusting. Whereas we cannot rule out this possibility on the basis of P-T-t data alone, we note that such large out-of-sequence thrusts have not yet been reported elsewhere in the Himalaya.

Surprisingly, although geochemically similar generations of monazite occur at both Langtang and Annapurna (i.e., early prograde, late prograde, and postanatectic), monazite ages along the Modi Khola appear older by several million years than reported at Langtang. The Main Central thrust sheet at Langtang records late prograde monazite growth 16–23 Ma and postanatectic cooling 13–16 Ma (Kohn et al., 2005), whereas Main Central thrust rocks at Annapurna record late prograde monazite growth 21–23 Ma but cooling 16–20 Ma. Rocks in the Langtang thrust sheet at Langtang, wholly within the Greater Himalayan sequence, record late prograde monazite growth 22–23 Ma and cooling 17–19 Ma (Kohn et al., 2005). This suggests that the Main Central thrust at Annapurna is temporally equivalent to the Langtang thrust at Langtang.

One explanation for the observed geochronological differences between the Main Central thrust at Annapurna and Langtang is the presence of a lateral ramp along strike (Fig. 9A). That is, the thrust plane cuts up section from west to east. Alternatively, the Langtang thrust and Main Central thrust shear zones could have died out laterally (Fig. 9A). Because each thrust surface represents the accumulation of strain over millions of years, and because thrust surfaces may have accommodated slip differently in different areas, the present-day distribution of lithologic packages (Greater Himalayan sequence Formations 1a, 1b, 1c, Lesser Himalayan sequence, etc.) may not uniquely elucidate temporal evolution of the thrust. That is, the Main Central thrust surface is defined on lithologic rather than chronologic criteria, and juxtaposition of Greater Himalayan sequence and Lesser Himalayan sequence rocks may have been diachronous along strike.

Assuming that the Main Central thrust at Annapurna and the Langtang thrust at Langtang were active at the same time (Fig. 9A), the thrusts could have followed several possible sequences to attain their current geometry. One possibility is that the thrust plane consistently cut upsection between Annapurna and Langtang, connected by a lateral ramp (Fig. 9B), so that the thrust surfaces followed a sequence of progressive underthrusting in both regions. This is consistent with older ages for the Bhanuwa thrust and Sinuwa thrust in Annapurna compared to the Langtang thrust in Langtang, and implies that the Munsiari thrust in the Annapurna region should be of similar age to the Main Central thrust at Langtang. Monazite is absent in Lesser Himalayan sequence rocks in our Modi Khola transect, so we could not test this hypothesis directly. A variation of this model suggests the same progression down to the Main Central thrust but protracted Main Central thrust transport at Annapurna coincident with movement at Langtang (Fig. 9C). Yet another alternative suggests concurrent movement of the Main Central thrust at Annapurna and Langtang thrust at Langtang along noncontinual thrust planes, and the initiation of a lateral ramp cutting downsection 16–17 Ma that juxtaposed already-cooled Bhanuwa thrust and Sinuwa thrust sheets coeval with initial movement along the Main Central thrust at Langtang (Fig. 9D).

Although large-scale diachroneity or out-of-sequence thrusting implied by Figure 9D has not been reported previously in the Himalaya, our ability to resolve geological events has only recently improved to a level that allows us to look at strain partitioning over million-year time scales and potentially distinguish previously unrecognized spatial and temporal hetero-

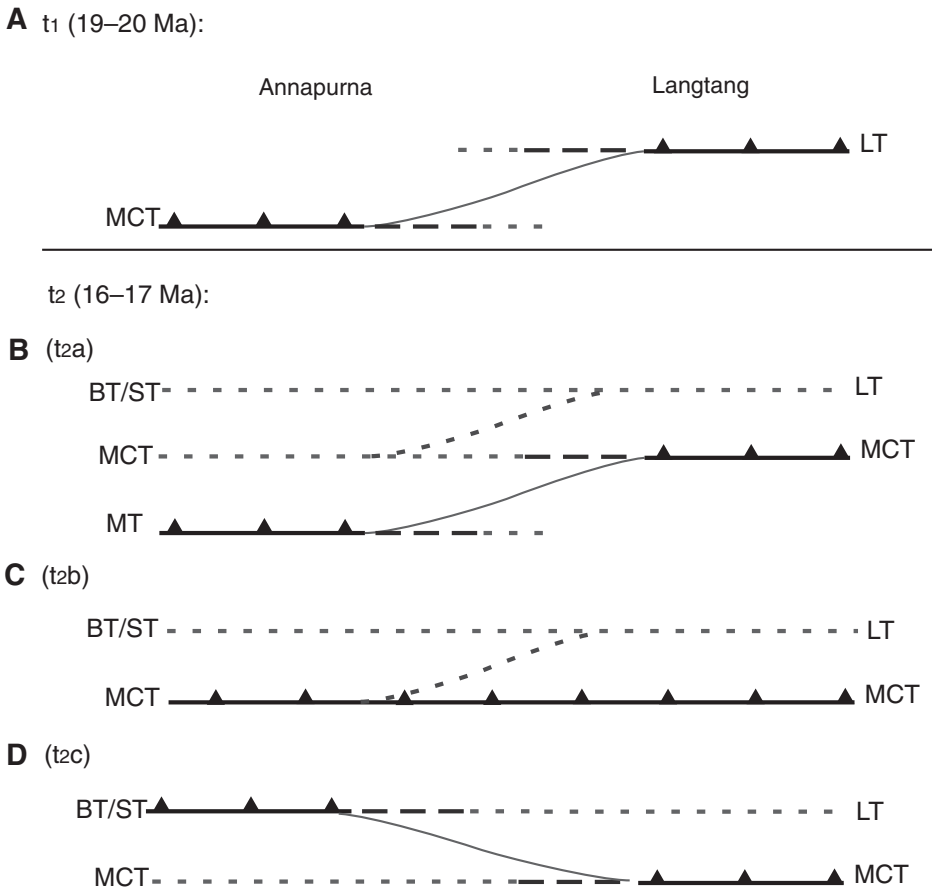

Figure 9. Schematic diagrams of thrust development. (A) t1 represents an initial geometry at 19–20 Ma in which the two thrusts in the Langtang and Annapurna areas either die out alongstrike (dashed and dotted lines), or have a lateral ramp connecting them (thin line). Potential progressions include: (B) continued underthrusting preserving the lateral ramp (t2a); (C) prolonged Main Central thrust (MCT) transport at Annupurna allowing in-sequence thrusting at Langtang to progress to the same tectonostratigraphic level (t2b); or (D) the development of a lateral ramp accommodating synchronous movement of cooled Bhanuwa thrust (BT) and Sinuwa thrust (ST) sheets at Annapurna (i.e., out-of-sequence thrusting) and a hot MCT sheet at Langtang (i.e., in-sequence thrusting). LT—Langtang thrust; MT—Munsiari thrust.

geneity. The data reveal a complexity that does not lead to a single solution, but nonetheless indicate that more work examining differences in strain partitioning on million-year or smaller time scales might elucidate previously unrecognized variabilities.

Despite differences in absolute ages, the similarities among the chemical systematics of monazite, peak P-T conditions, and thrust rates calculated for Langtang and Annapurna imply that strain measurements in one part of an orogen can be realistically extrapolated to another within a few hundred kilometers, although the timing of movement on discrete thrust surfaces may differ. This lateral predictability may hold only for geologically similar regions of the orogenic belt. With distance may come a change in boundary conditions that would prevent long-distance extrapolation of strain estimates. Additional comparable measurements from other parts of the orogen, e.g., in far eastern or western Nepal, India, and Bhutan, are needed to verify whether these results can be applied to the orogen as a whole.

ACKNOWLEDGMENTS

We thank N. McQuarrie and A. Martin for providing incisive reviews that helped us improve the manuscript significantly. J. Pyle and J. Price at Rensselaer Polytechnic Institute are thanked for assistance with the electron microprobe. A. Schmidt and P. Olin are thanked for their assistance with the ion microprobe at University of California–Los Angeles and the laser ablation–inductively coupled plasma mass spectrometer at Boise State. Discussions with M. Schmitz, C.J. Northrup, and D. Robinson greatly benefited the authors. F. Mazdab is thanked for sending the BLR-1 titanite standard. This material is based upon work supported by National Science Foundation grant numbers EAR-0073803, 0439733/0803549, and 0809428 to MJK.

APPENDIX: METHODS

Monazite grains were first identified in thin section using backscattered electron (BSE) imaging on the Cameca SX-100 electron microprobe housed in the Department of Earth and Environmental Sciences at Rensselaer Polytechnic Institute, Troy, New York. The monazite grains are all from the rock matrix, are typically zoned, and range in size from 20 to 300 µm. Monazite grains were X-ray mapped using the same electron microprobe (operating conditions below) to identify chemically distinct zones. They were then reidentified in thin section using an optical microscope, and, using a Medenbach microdrill, extracted from the slides in ~3-mm disks, preserving the textural relationship of the monazite grain with the surrounding matrix. The glass disks containing the monazites were then mounted in 1-inch epoxy rounds with a block of five to ten grains of polished standards (monazite 554, Harrison et al., 1999). To aid in locating the monazite for analyses, reflected light images were taken of each glass disk containing a monazite grain, as well as the entire epoxy round. The sample rounds were cleaned in distilled water in an ultrasonic bath, dried, and gold coated. Monazite grains were analyzed using the Cameca IMS 1270 ion microprobe in the Department of Earth and Space Sciences, University of California–Los Angeles.

Details of analytical protocols for $^{208}Pb/^{232}Th$ dating of monazite using the Cameca IMS 1270 ion microprobe have been described previously (Harrison et al., 1995, 1999). Operating conditions for this study involved a primary beam current of 6–10 nA, a spot size of 10–20 µm, and a mass resolving power of 4500, which sufficiently separates all molecular interferences in the 204 to 208 mass range. Energy offsets were +10 to +15 eV for $^{232}Th^+$, and –8 to –13 eV for ThO_2^+. Total time per spot analysis was 12 minutes. $^{208}Pb^+/Th^+$ was corrected for common Pb using the relationship $^{208}Pb^*/Th^+ = (^{208}Pb^+/Th^+)[1 - (^{208}Pb/^{204}Pb)_S(^{204}Pb^+/^{208}Pb^+)]$, where $(^{208}Pb/^{204}Pb)_S$ is the known ratio of the standard; the asterisk indicates the species is corrected for common Pb. The $^{208}Pb/^{232}Th$ relative sensitivity factor required to calculate a Th-Pb age from isotopic data obtained from an unknown monazite is determined by referring the ThO_2/Th ratio determined in the sample analysis to a linear calibration curve that is constructed from several ion microprobe spot measurements of ThO_2/Th versus $^{208}Pb/Th$ from standard monazite 554. This correction factor permits the determination of Pb/Th ratios of unknown grains measured under the same instrumental conditions. Reported age uncertainties reflect counting statistics and the reproducibility of the standard calibration curve.

Elemental compositions and X-ray maps were collected using the Cameca SX-100 electron microprobe housed in the Department of Earth and Environmental Sciences at Rensselaer Polytechnic Institute, Troy, New York. Natural and synthetic silicates and oxides were used for calibrations, and quantitative measurements were made using an accelerating voltage of 15 kV and a current of 20 nA. A minimum beam size was used on most minerals, except plagioclase and micas (10 µm), with peak count times of 10 s (Na, Ca, Fe, Mn, Si, Al) or 20 s (Mg, Ti, K). Operating conditions

for the X-ray maps consisted of an accelerating voltage of 15 kV, current of 200 nA, pixel time of 30 ms, minimum beam size, and step size of 2–5 µm/pixel. X-ray compositional maps of the elements Fe, Mg, Mn, Ca, and Al were collected on garnet, and Th, Y, U, Ce, and Ca on monazite. Garnet and monazite maps were collected via stage and beam mapping, respectively.

Trace-element compositions of titanite were measured using laser ablation ICP-MS at Boise State University. We used a Thermo XSeries2 Quadrupole ICP-MS, and a New Wave UP-213 laser (frequency quintupled Nd-YAG) operating at 5 Hz and 8–10 J/cm^2, as calibrated at the factory, and a 25-µm spot. A broad suite of major and trace elements were analyzed, most significantly for this work: Al, Si, Ca, Ti, Fe, and Zr. Count times were 3 ms on Al, 5 ms on Si, Ca, and Fe, 10 ms on Ti, and 20 ms on Zr. One hundred cycles through each set of elements were averaged. Calibrations were based on BLR-1 (Mazdab, 2009). Compositions were normalized to 30 wt% SiO_2 and are reported in Table DR5 (see footnote 1).

Peak temperature and pressure estimates were calculated via exchange reactions and thermodynamic equilibria. The garnet-biotite thermometer of Ferry and Spear (1978) with the Berman (1990) garnet solution model was used for most samples except AS01-41b, in which the garnet-chlorite thermometer of Dickenson and Hewitt (1986; modified in Laird, 1988) was used with the Berman (1990) garnet solution model. These calibrations give results consistent with phase equilibria elsewhere in the Himalaya (Kohn, 2008). In calc-silicates from Formation II, temperatures were estimated using the Zr-in-titanite thermometer of Hayden et al. (2008) at an assumed pressure of 10 kbar and activity of TiO_2 of 0.85 (e.g., see discussion of Corrie et al., 2010). Errors are reported for the internal consistency of Zr measurements; uncertainties of ±2 kbar in pressure and ±0.1 in the activity of TiO_2 contribute additional errors of ±30 and ±10 °C, respectively. Depending on the mineral assemblage of the sample, pressures were calculated using the barometers garnet-plagioclase-aluminosilicate-quartz (Koziol and Newton, 1988, with the Berman, 1990, garnet solution model), garnet-plagioclase-muscovite-biotite (Hoisch, 1990), or garnet-plagioclase-biotite-quartz (Hoisch, 1990). Different thermobarometric calibrations may shift the temperatures and pressures reported for each sample by as much as 25 °C and 1 kbar, but the major trends are preserved.

Appropriate mineral compositions were selected using standard petrologic criteria (e.g., Spear et al., 1990; Spear, 1991, 1993; Kohn et al., 1992, 1993; Kohn and Spear, 2000) to provide the best estimate of peak metamorphic conditions. The composition of garnet that most closely preserves peak metamorphic conditions is the composition nearest the rim that was least affected by retrograde reactions. In the Lesser Himalayan sequence, temperatures were sufficiently low that prograde garnet compositions are commonly retained, and compositions at or near the rim were selected. These garnet compositions were combined with compositions of plagioclase (when present), biotite, muscovite, and chlorite (only one sample) near the garnet that appeared to be texturally equilibrated, rather than retrograde products.

In the Greater Himalayan sequence, however, sufficiently high temperatures were reached that diffusion, retrograde exchange reactions (ReERs), or retrograde net transfer reactions (ReNTRs) either partially or entirely modified the original growth zoning in garnet, which can strongly influence calculated temperature and pressure (e.g., Spear, 1991; Kohn and Spear, 2000). A common method to estimate peak temperatures is to use the composition of garnet where Mn and Fe/(Fe + Mg) form a trough, that is, the composition nearest the rim that was least affected by retrograde reactions (Kohn et al., 1992, 1993; Kohn and Spear, 2000). In some cases where diffusional homogenization has occurred, this location is near the core of the garnet. However, pairing a garnet composition with a nearby biotite composition that has experienced Fe enrichment will cause the estimated temperatures to be too high (Kohn and Spear, 2000). Therefore, a correction must be made to the biotite composition to account for Fe enrichment due to garnet dissolution.

Using garnet X-ray maps to estimate the amount of dissolution of the garnet, the amount of Fe enrichment in biotite due to ReNTRs may be estimated, and the biotite compositions subsequently corrected (Kohn and Spear, 2000). In some samples, the correction to the biotite compositions was minor, and equivalent temperatures could be calculated by using compositions from biotite distal to the garnet that were not affected by ReNTRs. In other samples, correction to the biotite compositions lowered estimated temperatures 10 to 50 °C. To calculate P-T conditions in Greater Himalayan sequence samples, the garnet composition with the lowest Fe/(Fe + Mg) and Mn were chosen and combined with corrected or distal biotite (depending on the sample), proximal muscovite, and rim compositions of proximal plagioclase. Evidence to support the estimated P-T conditions includes agreement with the stability of observed mineral assemblages and consistency with P-T conditions of nearby samples that have different compositions.

REFERENCES CITED

Ahmad, T., Harris, N., Bickle, M., Chapman, H., Bunbury, J., and Prince, C., 2000, Isotopic constraints on the structural relationships between the Lesser Himalayan series and High Himalayan crystalline series, Garhwal Himalaya: Geological Society of America Bulletin, v. 112, p. 467–477, doi: 10.1130/0016-7606(2000)112<467:ICOTSR>2.0.CO;2.

Beaumont, C., Jamieson, R.A., Nguyen, M.H., and Lee, B., 2001, Himalayan tectonics explained by extrusion of a low-viscosity crustal channel coupled to focused surface denudation: Nature, v. 414, p. 738–742, doi: 10.1038/414738a.

Beaumont, C., Jamieson, R.A., Nguyen, M.H., and Medvedev, S., 2004, Crustal channel flows: 1. Numerical models with applications to the tectonics of the Himalayan-Tibetan orogen: Journal of Geophysical Research, v. 109, B06406, doi: 10.1029/2003JB002809.

Berman, R.G., 1990, Mixing properties of Ca-Mg-Fe-Mn garnets: The American Mineralogist, v. 75, p. 328–344.

Bettinelli, P., Avouac, J.-P., Flouzat, M., Jouanne, F., Bollinger, L., Willis, P., and Chitrakar, G.R., 2006, Plate motion of India and interseismic strain in the Nepal Himalaya from GPS and DORIS measurements: Journal of Geodesy, v. 80, p. 567–589, doi: 10.1007/s00190-006-0030-3.

Beyssac, O., Bollinger, L., Avouac, J.-P., and Goffe, B., 2004, Thermal metamorphism in the Lesser Himalaya of Nepal determined from Raman Spectroscopy of carbonaceous material: Earth and Planetary Science Letters, v. 225, p. 233–241, doi: 10.1016/j.epsl.2004.05.023.

Bilham, R., Larson, K., and Freymueller, J., 1997, Indo-Asian convergence rates in the Nepal Himalaya: Nature, v. 311, p. 621–626.

Bollinger, L., Henry, P., and Avouac, J.-P., 2006, Mountain building in the Nepal Himalaya: Thermal and kinetic model: Earth and Planetary Science Letters, v. 244, p. 58–71, doi: 10.1016/j.epsl.2006.01.045.

Bordet, P., 1961, Recherches Géologiques dans l'Himalaya du Népal, Région du Makalu: Paris, Centre National de la Recherches Scientifiques, 275 p.

Catlos, E.J., Harrison, T.M., Kohn, M.J., Grove, M., Ryerson, F.J., Manning, C.E., and Upreti, B.N., 2001, Geochronologic and thermobarometric constraints on the evolution of the Main Central thrust, central Nepal Himalaya: Journal of Geophysical Research, v. 106, p. 16177–16204, doi: 10.1029/2000JB900375.

Catlos, E.J., Gilley, L.D., and Harrison, T.M., 2002, Interpretation of monazite ages obtained via in situ analysis: Chemical Geology, v. 188, p. 193–215, doi: 10.1016/S0009-2541(02)00099-2.

Colchen, M., Le Fort, P., and Pêcher, A., 1986, Annapurna-Manaslu-Ganesh Himal: Paris, Centre National de la Recherches Scientifiques, 136 p.

Corrie, S.L., and Kohn, M.J., 2008, Trace-element distributions in silicates during prograde metamorphic reactions: Implications for monazite formation: Journal of Metamorphic Geology, v. 26, p. 451–464, doi: 10.1111/j.1525-1314.2008.00769.x.

Corrie, S.L., Kohn, M.J., and Vervoort, J.D., 2010, Young eclogite from the Greater Himalayan Sequence, Arun Valley, eastern Nepal: P-T-t path and tectonic implications: Earth and Planetary Science Letters, v. 289, p. 406–416, doi: 10.1016/j.epsl.2009.11.029.

Dahl, P.S., Hamilton, M.A., Jercinovic, M.J., Terry, M.P., Williams, M.L., and Frei, R., 2005, Comparative isotopic and chemical geochronometry of monazite, with implications for U-Th-Pb dating by electron microprobe: An example from metamorphic rocks of the eastern Wyoming craton (USA): The American Mineralogist, v. 90, p. 619–638, doi: 10.2138/am.2005.1382.

Daniel, C.G., Hollister, L.S., Parrish, R.R., and Grujic, D., 2003, Exhumation of the Main Central thrust from lower crustal depths, eastern Bhutan Himalaya: Journal of Metamorphic Geology, v. 21, p. 317–334, doi: 10.1046/j.1525-1314.2003.00445.x.

DeCelles, P.G., Gehrels, G.E., Quade, J., LaReau, B., and Spurlin, M., 2000, Tectonic implications of U-Pb zircon ages of the Himalayan orogenic belt in Nepal: Science, v. 288, p. 497–499, doi: 10.1126/science.288.5465.497.

DeCelles, P.G., Robinson, D.M., Quade, J., Ojha, T.P., Garzione, C.N., Copeland, P., and Upreti, B.N., 2001, Stratigraphy, structure, and tectonic evolution of the Himalayan fold-thrust belt in western Nepal: Tectonics, v. 20, p. 487–509, doi: 10.1029/2000TC001226.

DeCelles, P.G., Gehrels, G.E., Najman, Y., Martin, A.J., Carter, E., and Garzanti, E., 2004, Detrital geochronology and geochemistry of Cretaceous–early Miocene strata of Nepal: Implications for timing and diachroneity of initial Himalayan orogenesis: Earth and Planetary Science Letters, v. 227, p. 313–330, doi: 10.1016/j.epsl.2004.08.019.

Dickenson, M.P., and Hewitt, D., 1986, A garnet-chlorite geothermometer: Geological Society of America Abstracts with Programs, v. 18, p. 584.

Dunlap, W.J., Weinberg, R.F., and Searle, M.P., 1998, Karakoram fault zone rocks cool in two phases: Journal of the Geological Society, v. 155, p. 903–912, doi: 10.1144/gsjgs.155.6.0903.

Ferry, J.M., 2000, Patterns of mineral occurrence in metamorphic rocks: The American Mineralogist, v. 85, p. 1573–1588.

Ferry, J.M., and Spear, F.S., 1978, Experimental calibration of partitioning of Fe and Mg between biotite and garnet: Contributions to Mineralogy and Petrology, v. 66, p. 113–117, doi: 10.1007/BF00372150.

Florence, F.P., and Spear, F.S., 1991, Effects of diffusional modification of garnet growth zoning on P-T path calculations: Contributions to Mineralogy and Petrology, v. 107, p. 487–500, doi: 10.1007/BF00310683.

Foster, G., Kinny, P., Vance, D., Prince, C., and Harris, N., 2000, The significance of monazite U-Th-Pb age data in metamorphic assemblages: A combined study of monazite and garnet chronometry: Earth and Planetary Science Letters, v. 181, p. 327–340, doi: 10.1016/S0012-821X(00)00212-0.

Foster, G., Gibson, H.D., Parrish, R., Horstwood, M., Fraser, J., and Tindle, A., 2002, Textural, chemical and isotopic insights into the nature and behavior of metamorphic monazite: Chemical Geology, v. 191, p. 183–207, doi: 10.1016/S0009-2541(02)00156-0.

Foster, G., Parrish, R.R., Horstwood, M.S.A., Chenery, S., Pyle, J., and Gibson, H.D., 2004, The generation of prograde P-T-t points and paths: A textural, compositional, and chronological study of metamorphic

monazite: Earth and Planetary Science Letters, v. 228, p. 125–142, doi: 10.1016/j.epsl.2004.09.024.

Fraser, G., Worley, B., and Sandiford, M., 2000, High-precision geothermobarometry across the High Himalayan metamorphic sequence, Langtang Valley, Nepal: Journal of Metamorphic Geology, v. 18, p. 665–681, doi: 10.1046/j.1525-1314.2000.00283.x.

Ganguly, J., Cheng, W., and Tirone, M., 1996, Thermodynamics of an aluminosilicate garnet solid solution: New experimental data, an optimized model, and thermometry applications: Contributions to Mineralogy and Petrology, v. 126, p. 137–151.

Gehrels, G.E., DeCelles, P.G., Martin, A., Ojha, T.P., Pinhassi, G., and Upreti, B.N., 2003, Initiation of the Himalayan orogen as an early Paleozoic thin-skinned thrust belt: GSA Today, v. 13, p. 4–9, doi: 10.1130/1052-5173(2003)13<4:IOTHOA>2.0.CO;2.

Gehrels, G.E., DeCelles, P.G., Ojha, T.P., and Upreti, B.N., 2006, Geologic and U-Th_Pb geochronologic evidence for early Paleozoic tectonism in the Kathmandu thrust sheet, central Nepal Himalaya: Geological Society of America Bulletin, v. 118, p. 185–198, doi: 10.1130/B25753.1.

Gibson, H.D., Carr, S.D., Brown, R.L., and Hamilton, M.A., 2004, Correlations between chemical and age domains in monazite and metamorphic reactions involving major pelitic phases: An integration of ID-TIMS and SHRIMP geochronology with Y-Th-U X-ray mapping: Chemical Geology, v. 211, p. 237–260, doi: 10.1016/j.chemgeo.2004.06.028.

Grujic, D., Hollister, L.S., and Parrish, R.R., 2002, Himalayan metamorphic sequence as an orogenic channel: insight from Bhutan: Earth and Planetary Science Letters, v. 198, p. 177–191, doi: 10.1016/S0012-821X(02)00482-X.

Guillot, S., Garzanti, E., Baratoux, D., Marquer, D., Maheo, G., and de Sigoyer, J., 2003, Reconstructing the total shortening history of the NW Himalaya: Geochemistry, Geophysics, Geosystems, v. 4, doi: 10.1029/2002GC000484 (22).

Harrison, T.M., McKeegan, K.D., and Le Fort, P., 1995, Detection of inherited monazite in the Manaslu leucogranite by $^{208}Pb/^{232}Th$ ion microprobe dating: Crystallization age and tectonic implications: Earth and Planetary Science Letters, v. 133, p. 271–282, doi: 10.1016/0012-821X(95)00091-P.

Harrison, T.M., Ryerson, F.J., Le Fort, P., Yin, A., Lovera, O.M., and Catlos, E.J., 1997, A Late Miocene–Pliocene origin for central Himalayan inverted metamorphism: Earth and Planetary Science Letters, v. 146, p. E1–E7, doi: 10.1016/S0012-821X(96)00215-4.

Harrison, T.M., Grove, M., Lovera, O.M., and Catlos, E.J., 1998, A model for the origin on Himalayan anatexis and inverted metamorphism: Journal of Geophysical Research, v. 103, p. 27017–27032, doi: 10.1029/98JB02468.

Harrison, T.M., Grove, M., McKeegan, K.D., Coath, C.D., Lovera, O.M., and Le Fort, P., 1999, Origin and episodic emplacement of the Manaslu Intrusive Complex, central Himalaya: Journal of Petrology, v. 40, p. 3–19, doi: 10.1093/petrology/40.1.3.

Harrison, T.M., Catlos, E.J., and Montel, J.-M., 2002, U-Th-Pb dating of phosphate minerals: Reviews in Mineralogy, v. 48, p. 523–552.

Hayden, L.A., Watson, E.B., and Wark, D.A., 2008, A thermobarometer for sphene (titanite): Contributions to Mineralogy and Petrology, v. 155, p. 529–540, doi: 10.1007/s00410-007-0256-y.

Henry, P., Le Pichon, X., and Goffé, B., 1997, Kinematic, thermal and petrological model of the Himalayas: Constraints related to metamorphism within the underthrust Indian crust and topographic elevation: Tectonophysics, v. 273, p. 31–56, doi: 10.1016/S0040-1951(96)00287-9.

Herman, F., Copeland, P., Avouac, J.-P., Bollinger, L., Mahéo, G., Le Fort, P., Rai, S., Foster, D., Pêcher, A., Stüwe, K., and Henry, P., 2010, Exhumation, crustal deformation, and thermal structure of the Nepal Himalaya derived from the inversion of thermochronological and thermobarometric data and modeling of the topography: Journal of Geophysical Research, v. 115, p. B06407, doi: 10.1029/2008JB006126.

Hodges, K.V., Parrish, R.R., and Searle, M.P., 1996, Tectonic evolution of the central Annapurna Range, Nepalese Himalayas: Tectonics, v. 15, p. 1264–1291, doi: 10.1029/96TC01791.

Hoisch, T.D., 1990, Empirical calibration of six geobarometers for the mineral assemblage quartz + muscovite + biotite + plagioclase + garnet: Contributions to Mineralogy and Petrology, v. 104, p. 225–234, doi: 10.1007/BF00306445.

Hubbard, M.S., and Harrison, T.M., 1989, $^{40}Ar/^{39}Ar$ age constraints on deformation and metamorphism in the Main Central thrust zone and Tibetan slab, eastern Nepal Himalaya: Tectonics, v. 8, p. 865–880, doi: 10.1029/TC008i004p00865.

Huerta, A.D., Royden, L.H., and Hodges, K.V., 1998, The thermal structure of collisional orogens as a response to accretion, erosion, and radiogenic heating: Journal of Geophysical Research, v. 103, p. 15287–15302, doi: 10.1029/98JB00593.

Huerta, A.D., Royden, L.H., and Hodges, K.V., 1999, The effects of accretion, erosion, and radiogenic heat on the metamorphic evolution of collisional orogens: Journal of Metamorphic Geology, v. 17, p. 349–366, doi: 10.1046/j.1525-1314.1999.00204.x.

Inger, S., and Harris, N.B.W., 1992, Tectonothermal evolution of the High Himalaya crystalline sequence, Langtang Valley, northern Nepal: Journal of Metamorphic Geology, v. 10, p. 439–452, doi: 10.1111/j.1525-1314.1992.tb00095.x.

Jamieson, R.A., Beaumont, C., Nguyen, M.H., and Lee, B., 2002, Interaction of metamorphism, deformation, and exhumation in large convergent orogens: Journal of Metamorphic Geology, v. 20, p. 9–24, doi: 10.1046/j.0263-4929.2001.00357.x.

Jamieson, R.A., Beaumont, C., Medvedev, S., and Nguyen, M.H., 2004, Crustal channel flows: 2. Numerical models with implications for metamorphism in the Himalayan-Tibetan orogen: Journal of Geophysical Research, v. 109, B06407, doi: 10.1029/2003JB002811.

Johnson, M.R.W., Oliver, G.J.H., Parrish, R.R., and Johnson, S.P., 2001, Synthrusting metamorphism, cooling, and erosion of the Himalayan Kathmandu Complex, Nepal: Tectonics, v. 20, p. 394–415, doi: 10.1029/2001TC900005.

Kaneko, Y., 1995, Thermal structure in the Annapurna region, central Nepal Himalaya: Implication for the inverted metamorphism: Journal of Mineralogy, Petrology, and Economic Geology, v. 90, p. 143–154, doi: 10.2465/ganko.90.143.

Kohn, M.J., 2004, Oscillatory- and sector-zoned garnets record cyclic (?) rapid thrusting in central Nepal: Geochemistry, Geophysics, Geosystems, v. 5, p. Q12014, doi: 10.1029/2004GC000737.

Kohn, M.J., 2008, P-T-t data from central Nepal support critical taper and repudiate large-scale channel flow of the Greater Himalayan sequence: Geological Society of America Bulletin, v. 120, p. 259–273, doi: 10.1130/B26252.1.

Kohn, M.J., and Malloy, M.A., 2004, Formation of monazite via prograde metamorphic reactions among common silicates: Implications for age determinations: Geochimica et Cosmochimica Acta, v. 68, p. 101–113, doi: 10.1016/S0016-7037(03)00258-8.

Kohn, M.J., and Parkinson, C.D., 2002, Petrologic case for Eocene slab breakoff during the Indo-Asian collision: Geology, v. 30, p. 591-594.

Kohn, M.J., and Spear, F.S., 2000, Retrograde Net Transfer Reaction (ReNTR) Insurance for P-T Estimates: Geology, v. 28, p. 1127–1130, doi: 10.1130/0091-7613(2000)28<1127:RNTRIF>2.0.CO;2.

Kohn, M.J., Orange, D.L., Spear, F.S., Rumble, D., and Harrison, T.M., 1992, Pressure, temperature, and structural evolution of west-central New Hamphsire: Hot thrusts over cold basement: Journal of Petrology, v. 33, p. 521–556.

Kohn, M.J., Spear, F.S., and Dalziel, I.W.D., 1993, Metamorphic P-T paths from Cordillera Darwin, a core complex in Tierra del Fuego, Chile: Journal of Petrology, v. 34, p. 519–542.

Kohn, M.J., Catlos, E.J., Ryerson, F.J., and Harrison, T.M., 2001, Pressure-temperature-time path discontinuity in the Main Central thrust zone, central Nepal: Geology, v. 29, p. 571–574, doi: 10.1130/0091-7613(2001)029<0571:PTTPDI>2.0.CO;2.

Kohn, M.J., Wieland, M., Parkinson, C.D., and Upreti, B.N., 2004, Miocene faulting at plate tectonic velocity in the Himalaya of central Nepal: Earth and Planetary Science Letters, v. 228, p. 299–310, doi: 10.1016/j.epsl.2004.10.007.

Kohn, M.J., Wieland, M., Parkinson, C.D., and Upreti, B.N., 2005, Five generations of monazite in Langtang gneisses: Implications for geochronology of the Himalayan metamorphic core: Journal of Metamorphic Geology, v. 23, p. 399–406, doi: 10.1111/j.1525-1314.2005.00584.x.

Kohn, M.J., Paul, S.K., and Corrie, S.L., 2010, The lower Lesser Himalayan sequence: A Paleoproterozoic arc on the northern margin of the Indian plate: Geological Society of America Bulletin, v. 122, p. 323–335, doi: 10.1130/B26587.1.

Koziol, A.M., and Newton, R.C., 1988, Redetermination of the anorthite breakdown reaction and improvement of the plagioclase-garnet-Al_2SiO_5-quartz geobarometer: The American Mineralogist, v. 73, p. 216–223.

Laird, J., 1988, Chlorites: Metamorphic petrology. Hydrous phyllosilicates (exclusive of micas): Reviews in Mineralogy, v. 19, p. 405–453.

Larson, K.M., Bürgmann, R., Bilham, R., and Freymueller, J.T., 1999, Kinematics of the India- Eurasia collision zone from GPS measurements: Journal of Geophysical Research, v. 104, p. 1077–1093, doi: 10.1029/1998JB900043.

Lavé, J., and Avouac, J.P., 2001, Fluvial incision and tectonic uplift across the Himalaya of central Nepal: Journal of Geophysical Research, v. 106, p. 26,561–26,591, doi: 10.1029/2001JB000359.

Le Fort, P., 1975, Himalaya, the collided range, present knowledge of the continental arc: American Journal of Science, v. 275A, p. 1–44.

Long, S., McQuarrie, N., Tobgay, T., and Grujic, D., 2011, Geometry and crustal shortening of the Himalayan fold-thrust belt, eastern and central Bhutan: Geological Society of America Bulletin, doi: 10.1130/B30203.1 (in press).

Macfarlane, A.M., 1993, The chronology of tectonic events in the crystalline core of the Himalaya, Langtang National Park, central Nepal: Tectonics, v. 12, p. 1004–1025, doi: 10.1029/93TC00916.

Macfarlane, A.M., 1995, An evaluation of the inverted metamorphic gradient at Langtang National Park, central Nepal Himalaya: Journal of Metamorphic Geology, v. 13, p. 595–612, doi: 10.1111/j.1525-1314.1995.tb00245.x.

Martin, A.J., DeCelles, P.G., Gehrels, G.E., Patchett, P.J., and Isachsen, C., 2005, Isotopic and structural constraints on the location of the Main Central thrust in the Annapurna Range, central Nepal Himalaya: Geological Society of America Bulletin, v. 117, p. 926–944, doi: 10.1130/B25646.1.

Martin, A.J., Gehrels, G.E., and DeCelles, P.G., 2007, The tectonic significance of (U,Th)/Pb ages of monazite inclusions in garnet from the Himalaya of central Nepal: Chemical Geology, v. 244, p. 1–24, doi: 10.1016/j.chemgeo.2007.05.003.

Martin, A.J., Ganguly, J., and DeCelles, P.G., 2010, Metamorphism of Greater and Lesser Himalayan rocks exposed in the Modi Khola valley, central Nepal: Contributions to Mineralogy and Petrology, v. 159, p. 203–223, doi: 10.1007/s00410-009-0424-3.

Mazdab, F.K., 2009, Characterization of flux-grown trace-element-doped titanite using the high-mass-resolution ion microprobe (SHRIMP-RG): Canadian Mineralogist, v. 47, p. 813–831, doi: 10.3749/canmin.47.4.813.

McDougall, I., and Harrison, T.M., 1999, Geochronology and thermochronology by the $^{40}Ar/^{39}Ar$ method: Oxford, Oxford University Press, 269 p.

Overstreet, W.C., 1967, The geologic occurrence of monazite: U.S. Geological Survey Professional Paper 530, 327 p.

Parrish, R.R., 1990, U-Pb dating of monazite and its application to geological problems: Canadian Journal of Earth Sciences, v. 27, p. 1431–1450.

Parrish, R.R., and Hodges, K.V., 1996, Isotopic constraints on the age and provenance of the Lesser and Greater Himalayan sequences, Nepalese Himalaya: Geological Society of America Bulletin, v. 108, p. 904–911,

doi: 10.1130/0016-7606(1996)108<0904:ICOTAA>2.3.CO;2.

Pearson, O.N., and DeCelles, P.G., 2005, Structural geology and regional tectonic significance of the Ramgarh thrust, Himalayan fold-thrust belt of Nepal: Tectonics, v. 24, p. TC4008, doi: 10.1029/2003TC001617.

Pêcher, A., and Le Fort, P., 1986, The metamorphism in central Himalaya, its relations with the thrust tectonics, *in* Le Fort, P., Colchen, M., and Montenat, C., eds., Évolution des domains orogéniques d'Asie méridionale (de la Turquie à l'Indoneasie): Science de la Terre, v. 47, p. 285–309.

Pyle, J.M., and Spear, F.S., 1999, Yttrium zoning in garnet: Coupling of major and accessory phases during metamorphic reactions: Geological Materials Research, v. 1, p. 2–49.

Pyle, J.M., and Spear, F.S., 2003, Four generations of accessory-phase growth in low-pressure migmatites from SW New Hampshire: The American Mineralogist, v. 88, p. 338–351.

Pyle, J.M., Spear, F.S., Rudnick, R.L., and McDonough, W.F., 2001, Monazite-xenotime-garnet equilibrium in metapelites and a new monazite-garnet thermometer: Journal of Petrology, v. 42, p. 2083–2107, doi: 10.1093/petrology/42.11.2083.

Pyle, J.M., Spear, F.S., Cheney, J.T., and Layne, G., 2005, Monazite ages in the Chesham Pond Nappe, SW New Hampshire, USA: Implications for assembly of central New England thrust sheets: The American Mineralogist, v. 90, p. 592–606, doi: 10.2138/am.2005.1341.

Richards, A., Argles, T., Harris, N., Parrish, R., Ahmad, T., Darbyshire, F., and Draganits, E., 2005, Himalayan architecture constrained by isotopic tracers from clastic sediments: Earth and Planetary Science Letters, v. 236, p. 773–796, doi: 10.1016/j.epsl.2005.05.034.

Richards, A., Parrish, R., Harris, N., Argles, T., and Zhang, L., 2006, Correlation of lithotectonic units across the eastern Himalaya, Bhutan: Geology, v. 34, p. 341–344, doi: 10.1130/G22169.1.

Robinson, D.M., DeCelles, P.G., Patchett, P.J., and Garzione, C.N., 2001, The kinematic evolution of the Nepalese Himalaya interpreted from Nd isotopes: Earth and Planetary Science Letters, v. 192, p. 507–521, doi: 10.1016/S0012-821X(01)00451-4.

Robinson, D.M., DeCelles, P.G., Garzione, C.N., Pearson, O.N., Harrison, T.M., and Catlos, E.J., 2003, Kinematic model for the Main Central thrust in Nepal: Geology, v. 31, p. 359–362, doi: 10.1130/0091-7613(2003)031<0359:KMFTMC>2.0.CO;2.

Robinson, D.M., DeCelles, P.G., and Copeland, P., 2006, Tectonic evolution of the Himalayan thrust belt in western Nepal: Implications for channel flow models: Geological Society of America Bulletin, v. 118, p. 865–885, doi: 10.1130/B25911.1.

Searle, M.P., Law, R.D., Godin, L., Larson, K.P., Streule, M.J., Cottle, J.M., and Jessup, M.J., 2008, Defining the Himalayan Main Central thrust in Nepal: Journal of the Geological Society of London, v. 165, p. 523–534, doi: 10.1144/0016-76492007-081.

Spear, F.S., 1991, On the interpretation of peak metamorphic temperatures in the of garnet diffusion during cooling: Journal of Metamorphic Geology, v. 9, p. 379–388, doi: 10.1111/j.1525-1314.1991.tb00533.x.

Spear, F.S., 1993, Metamorphic phase equilibria and pressure-temperature-time paths: Washington, D.C., Mineralogical Society of America, 799 p.

Spear, F.S., and Markussen, J.C., 1997, Mineral zoning, P-T-X-M phase relations, and metamorphic evolution of some Adirondack granulites, New York: Journal of Petrology, v. 38, p. 757–783.

Spear, F.S., and Pyle, J.M., 2002, Apatite, monazite and xenotime in metamorphic rocks: Reviews in Mineralogy, v. 48, p. 293–335, doi: 10.2138/rmg.2002.48.7.

Spear, F.S., Kohn, M.J., Florence, F.P., and Menard, T., 1990, A model for garnet and plagioclase growth in pelitic schists: Implications for thermobarometry and P-T path determinations: Journal of Metamorphic Geology, v. 8, p. 683–696, doi: 10.1111/j.1525-1314.1990.tb00495.x.

Vannay, J.-C., and Hodges, K.V., 1996, Tectonomorphic evolution of the Himalayan metamorphic core between the Annapurna and Dhaulagiri, central Nepal: Journal of Metamorphic Geology, v. 14, p. 635–656, doi: 10.1046/j.1525-1314.1996.00426.x.

Vernon, R.H., 1979, Formation of late sillimanite by hydrogen metasomatism (base-leaching) in some high-grade gneisses: Lithos, v. 12, p. 143–152, doi: 10.1016/0024-4937(79)90045-8.

Wing, B.A., Ferry, J.M., and Harrison, T.M., 2003, Prograde destruction and formation of monazite and allanite during contact and regional metamorphism of pelites: Petrology and geochronology: Contributions to Mineralogy and Petrology, v. 145, p. 228–250, doi: 10.1007/s00410-003-0446-1.

Yin, A., 2006, Cenozoic tectonic evolution of the Himalayan orogen as constrained by along-strike variation of structural geometry, exhumation history, and foreland sedimentation: Earth-Science Reviews, v. 76, p. 1–131, doi: 10.1016/j.earscirev.2005.05.004.

Yin, A., and Harrison, T.M., 2000, Geologic evolution of the Himalayan-Tibet orogen: Annual Review of Earth and Planetary Sciences, v. 28, p. 211–280, doi: 10.1146/annurev.earth.28.1.211.

Science Editor: Christian Koeberl
Associate Editor: Moonsup Cho

Manuscript Received 29 July 2010
Revised Manuscript Received 26 October 2010
Manuscript Accepted 28 October 2010

Printed in the USA